Chapter 5

Sequential nucleation and growth of complex nanostructures

§ 5.1 Introduction

Although self assembly has occurred in nature for thousands of years (for instance, the formation of salt crystals and the intricate structure of snowflakes), the term 'self assembly' as used in chemical synthesis is relative new. Self assembly refers to the creation by physical or chemical reaction of small building units, which may be nanoparticles (NPs), nanorods (NRs), *etc*, which then aggregate together in specific arrangements to give one-dimensional (1D), two-dimensional (2D) or even three-dimensional (3D) superstructures [1]. The aggregation may be spontaneous without human intervention, or may be as a result of changing local conditions, *e.g.* temperature, concentration, drying, *etc*. Current understanding extends only to the most rudimentary of these stages for its use in materials, biology, chemistry, and condensed matter science [2].

Self-assembled nanostructures are new forms of materials which are interesting from a fundamental scientific perspective, as well as having many potential technological applications [3,4,5]. The rapid expansion of research work in this area is driven by the need to further miniaturize electronic components. Another reason is that, at the nanoscale, material properties are quite different from those of the bulk, and are strongly size-dependent. It is possible to process materials which can be tuned via size control to achieve specific functionality. In nanocrystals, the effect of

the surface is comparable in some cases to the chemical composition in influencing the chemical, electronic, magnetic and optical behaviours.

Due to the emergence of a new generation of high-technology materials, 2D and 3D self-assembled, aligned nanomaterials have begun to be widely investigated over the last decade [6,7]. It is believed that the ability of nanostructures to self-assemble with controlled crystalline orientation, size, complexity and crystal morphology provide potential applications in data storage, functional devices, communications and technology. As a result, a rapidly growing field of science has emerged to understand and control these self-organized architectures, involving the dedicated efforts of chemists, physicists, material scientists and biologists. In general, physical methods (including chemical vapor deposition [8], vapour phase transport [9], and pulsed laser ablation in vacuum [10]) and chemical methods (including hydrothermal methods [11], soft-template [12] and use of various surfactants [13,14]) have been developed to fabricate nano- to microscale materials with a range of morphologies, such as compact hexagonal networks [15], rings [16], dandelion-shaped hollow structures [17], strips [18], tubes [19], and flower-like structures [20]. For example, ZnO forms micron- and submicron-scale 'dandelion'-like structures (Figure 5.1(a)), which are comprised of single-crystalline building units (either NRs or NPs) [21], and which can be constructed via a modified Kirkendall process in solution, where the pre-formed oxide layer serves as a shell template for the initial nucleation and growth. Also, uniform Sb_2S_3 bundles coalesced from numerous NRs (Figure 5.1(b)) have been synthesized on a large scale using a hydrothermal technique, at a temperature of 180°C for 20 h [22]. However, It is well known that these physical techniques require relatively high temperature, vacuum conditions, and expensive equipment, or sometimes complicated processes, which limit them to smaller scale fabrication. Also, conventional chemical methods usually involve the use of catalysts, surfactants and possibly complex chemical reactions, which often produce a significant amount of unwanted byproducts requiring further purification. Therefore, a technique which combines the merits of both physical and chemical methods, while giving high yield at low cost, would be desirable, if novel self-assembled materials are to be produced on an industrial scale.

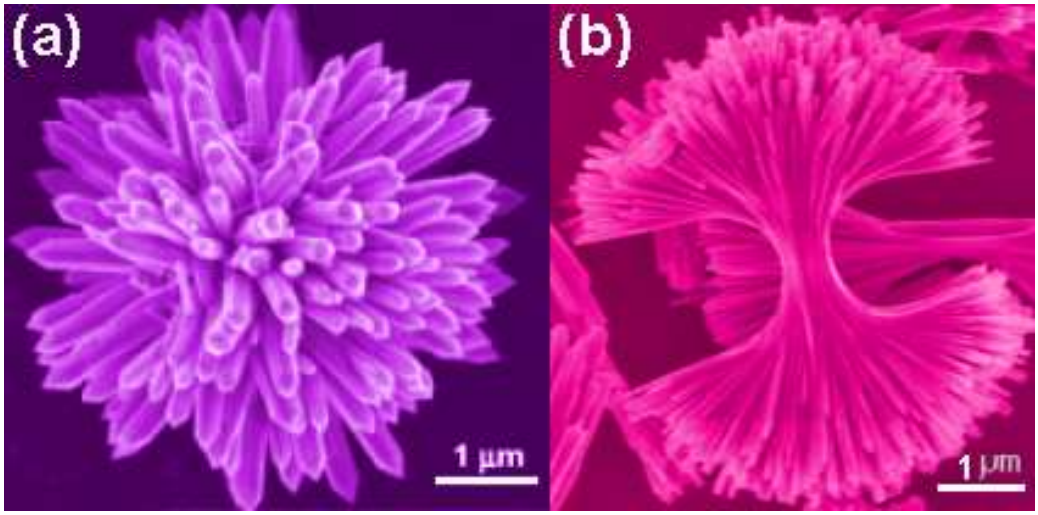

Figure 5.1 (a) ZnO 'dandelions' formed from ZnO NRs [21]. (b) Uniform Sb_2S_3 bundles formed from the coalescence of numerous NRs [22].

One such technique, liquid-phase pulsed laser ablation (LP-PLA), has only relatively recently been applied to produce self-organized nanomaterials [23,24,25]. Details about the technical aspects of LP-PLA can be seen in Chapter 2. Briefly, LP-PLA involves focusing a high power laser beam onto the surface of a solid target, which is submerged beneath a liquid. The interaction of the laser with the target causes the surface to vaporise in the form of an ablation plume, which contains species such as atoms, ions, and clusters, travelling with high kinetic energy. The species in the plume collide and react with molecules of the surrounding liquid, producing new compounds containing atoms from both the original target and the liquid. Due the intensity of the laser and the nanosecond timescales, the instantaneous temperatures and pressures within the reaction volume can be extreme (many thousands of K at tens of GPa) [26]. Such high temperature, high pressure, and high density conditions provide a 'brute force' method of synthesising novel materials that have hitherto been inaccessible using milder, more conventional techniques.

Extensive progress towards many types of inorganic nanoparticles has been well investigated including metals, metal oxides, and other semiconductors [27]. However, to date, research on the understanding of the self-assembly processes of

Group IV-V compounds, such as carbon nitride, is still in its infancy, and synthesis of complex nanostructures has only just begun. Carbon nitride has been the subject of numerous publications since the prediction by Liu and Cohen [28] in 1989 that crystalline C_3N_4 should have superhard properties. However, a successful synthesis of bulk amounts of this material still remains a challenge. The synthesis difficulties are due to its low thermodynamic stability and complex bonding environment. Recently Li and co-workers [29] demonstrated a range of self-assembled carbon nitride morphologies (including nanotube bundles, aligned nanoribbons and microspheres) can be prepared by a solvothermal technique. Also, our recent findings [30] indicated that the instantaneous high temperature, high pressure and high density conditions that arise when a high-intensity focused laser beam impinges upon a graphite target confined by a thin layer of liquid ammonia can promote growth of crystalline carbon nitride NPs. In this chapter, we will further demonstrate a successful synthesis of carbon nitride hierarchical nanostructures via LP-PLA based on previous results (Chapter 4), whereby the nanocrystals self-assemble into complex 3D superstructures. Fabrication of these 3D carbon nitride structures from small building blocks via self-organization suggests that the chemical and physical properties of these superstructures are intrinsic to the self-assembly induced by the close vicinity of the NPs or NRs. Finally, a summary and expectation are discussed with regard to the application of LP-PLA as a synthesis route for highly desirable complex architectures.

§ 5.2 Processing hierarchically structured nanomaterials

Production of 0D NPs and 1D nanocrystals by laser ablation in liquid media has been extensively studied [31,32,33]. Since the 0D and 1D nanocrystals can serve as building blocks in forming 2D or 3D complex architectures with long term periodic structures, it should be expected that the LP-PLA approach would have great potential as a means to grow large arrays of hierarchical, complex, oriented and ordered superstructures. Extending this concept, we performed a two-step synthesis to produce oriented carbon nitride nanostructures based on previous results. In a

typical synthesis process, the carbon nitride seed solution was initially prepared by LP-PLA as discussed in Chapter 4. Secondly, the seed solution was physically deposited onto a 1 cm×1 cm silicon p-(100) substrate. Many more complex nanostructures than the simple NPs and NRs described in Chapter 4 can be produced in a controlled fashion by simply altering the drying time and drying method of the suspension of ablated product. Details of the drying procedure are given in Chapter 3.2.

§ 5.2.1 Structure of the nanocrystal self-assembly

Studies performed at various conditions showed that factors such as ablation time, laser energy, ammonia concentration and the drying speed were important in order to obtain organized assemblies of NPs. By depositing the carbon nitride seed solution onto a silicon substrate and controlling the drying process under different conditions, four main classes of structure were identified in the ablation product, categorised based upon their shape and size (Figure 5.2(a)). The first class of structure had the shape of thin plates with rounded edges. Since they were the components of the larger 'flower-like' structures (described later), they have been termed 'nano-petals'. The quantity of these nanopetals and their location with respect to the larger structures (see later) were dependent upon the deposition and drying conditions. As shown in Figure 5.2(b-c), this indicated that these nano-petals were 2D aligned crystallites of carbon nitride which preferentially aligned themselves perpendicularly to the surface of the Si substrate. The number and length of these nano-petals increased with increasing laser ablation time from 0.5 to 2 h for the same laser fluence. X-ray diffraction (XRD) analysis of these nano-petals showed that they were crystalline, and all the diffraction peaks were consistent with (*h*00) preferential orientation, as shown in Figure 5.3. The crystallographic information was indexed to hexagonal β-C_3N_4 ($P6_3/m$ (176)) with lattice constants $a_0 = 6.4017$ Å and $c_0 = 2.4041$ Å [34]. Interestingly, it is also possible that these nano-petals began to aggregate and self-assemble (Figure 5.2(d)). When the concentration of nano-petals in the suspension increased, they tried to minimize their interfacial energy upon subsequent drying of the liquid by preferential tilting with

respect to each other. This produced the second class of nanostructure, which has a 'grass-like' shape and exhibits several different morphologies (see later discussion). However, all are produced in large quantities and cover the whole substrate.

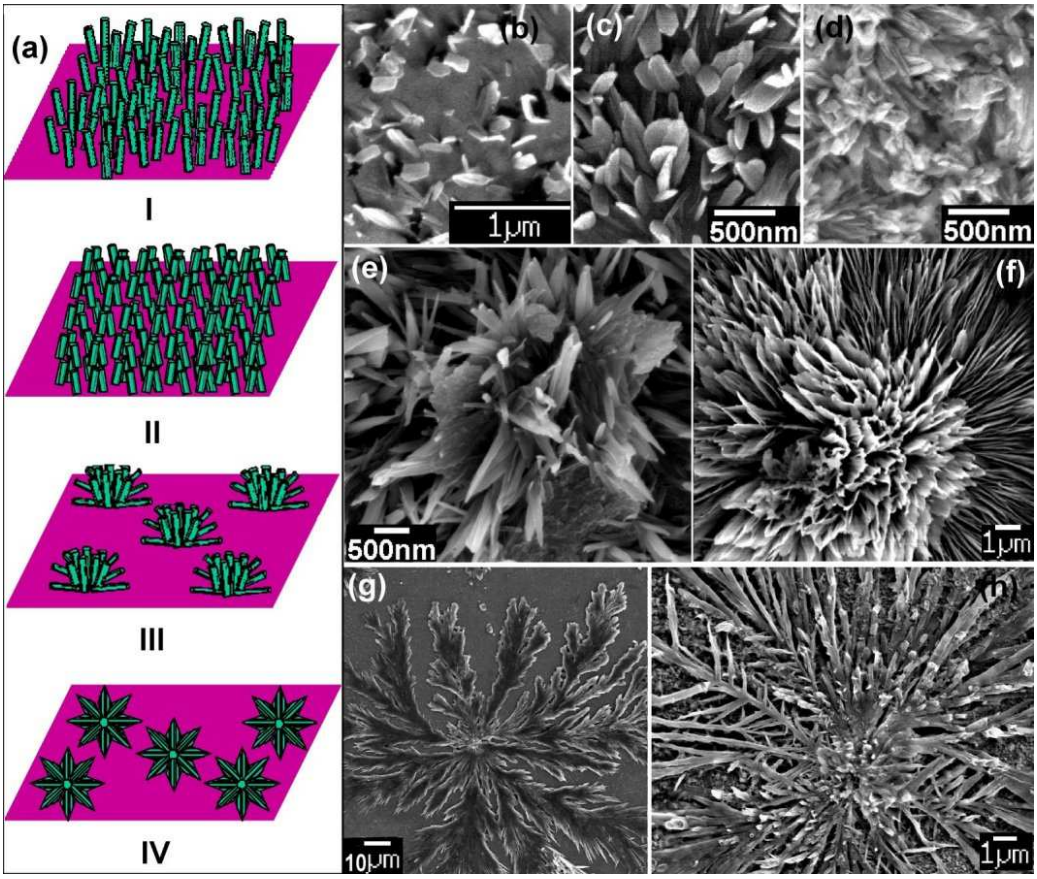

Figure 5.2 (a) Schematic illustration of the growth process leading to the observed four main classes of hierarchical structures, labelled I to IV. (b)-(d) Scanning electron microscopy (SEM) images of carbon nitride 'nano-petals' following ablation times of: (b) 0.5 h, (c) 2 h, and (d) 3 h. (e-f) Overall 'flower-like' structure following 5 h laser irradiation (synthesis conditions: laser power 125 mJ, 35% ammonia solution, drying in air). (g-h) 2D flattened flower, sample conditions identical to (e-f) except it was dried on a hotplate at 200ºC (g) and an oven 80ºC (h).

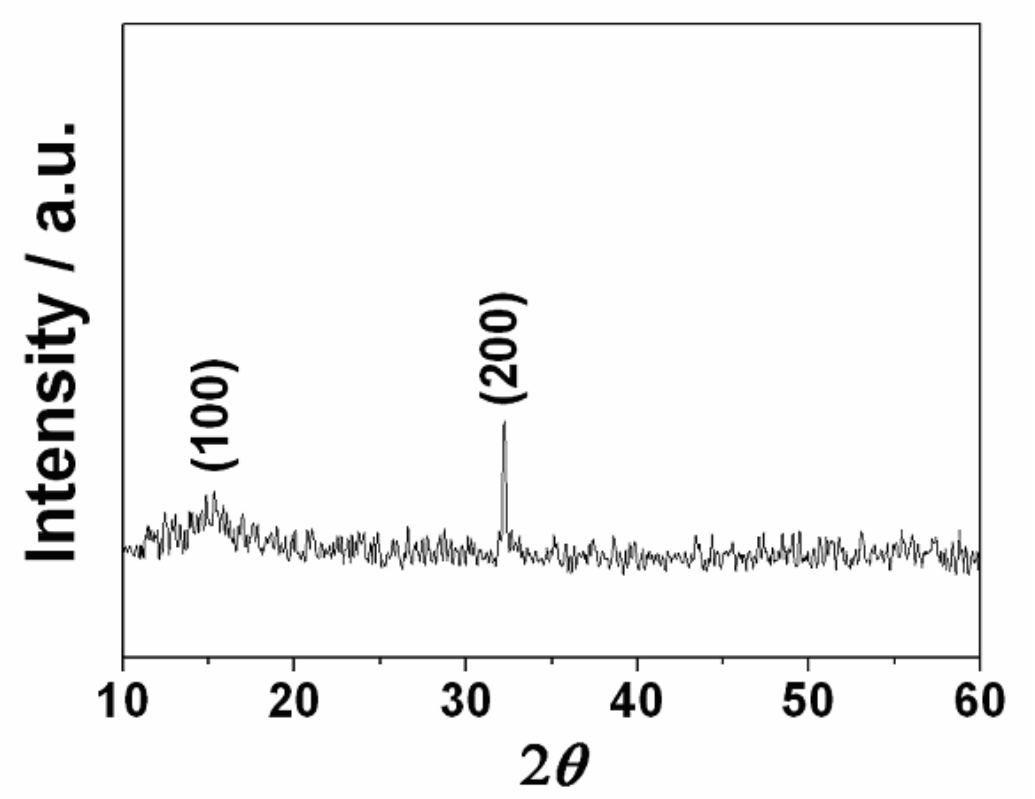

Figure 5.3 Representative XRD pattern of carbon nitride nanopetals prepared by LP-PLA (synthesis condition as Figure 5.2(c)).

By carefully controlling the drying process, 'flower-like' spiked, crystalline superstructures were formed (Figure 5.2(e-f)). This third class of structure, now fully 3-dimensional, with sizes 1-20 μm, were created when many nano-petal structures coalesced at a common centre with multi-fold symmetry. One possible explanation is that the presence of the solid substrate physically hinders growth in that direction; so many branches are tilted away from the substrate, towards the solution.

When the evaporation speed of the liquid was rapid (for example, drying in an oven or hotplate), a fourth class of structure was observed (Figure 5.2(g-h)). Instead of 3D flowers, the carbon nitride now formed 2D 'star-like' or flattened flower-like structures. New dendrites emanated from the core and acted as nucleation centres, eventually allowing the structure to expand into 2D horizontal flowers (Figure 5.2(h)). It is suggested that the higher water evaporation rate increased the

interparticle capillary forces [35]. As the continuous flux of particles filled up the spaces on the substrate, successive layers would be formed rather than 3D complex shapes.

Although these four kinds of structures have different densities and morphologies, they all exhibit high surface-to-volume ratios and so might have potential in semiconductor devices, anticorrosion protective coatings and new applications.

By controlling the solution evaporation rate on a carbon-coated TEM copper grid (as our substrate), different final complex architectures could be also achieved on various length scales. If the droplet dried in air (less than 1 h), the structure had the shape of nearly monodispersed spheres with rounded edges (Figure 5.4(a)). Those spheres have very high density and are close-packed. When increasing the laser fluence and ablation time, the nanostructure resembles 'flower-like' spiked crystallites (Figure 5.4(b)) for the same drying speed, where the NRs have coalesced at a common centre with multi-fold symmetry. It seems that these flower-like structures are simply less dense versions of the spheres (Figure 5.4(c)), with numerous voids between the NR framework comprising the flowers. Similar interior space would be eventually generated within the solids, as the smaller NPs are undergoing mass transport throughout the prolonging drying times (Figure 5.4(d)). The solid carbon nitride flower (similar to that in Figure 5.4(b)) has become hollow (named as 'hollow-flowers'), which divided the pristine solid sphere into two discrete regions and formed a core-shell structure. In these structures, the NPs have remain loosely attached to the outside, forming the interconnected void space, although the interior vacant volume might vary in each individual hollow-flower (for instance the interior void space size in order: 1st >2nd >3rd >4th, as shown colour contrast for two discrete regions of individual hollow-flower in Figure 5.4(d)). It is worth pointing out that by simply altering the drying time and drying method of the suspension, the final morphology can exhibit semi-hollow, core-shell, or even full-hollow structures. These observations are similar to the report by Liu and Zeng [36], who demonstrated the fabrication of ZnS nanomaterials with hollow interiors. Yang and Zeng also reported a simple approach to prepare hollow TiO_2 nanospheres with highly organized crystallites in the shell structure and surface regions [11].

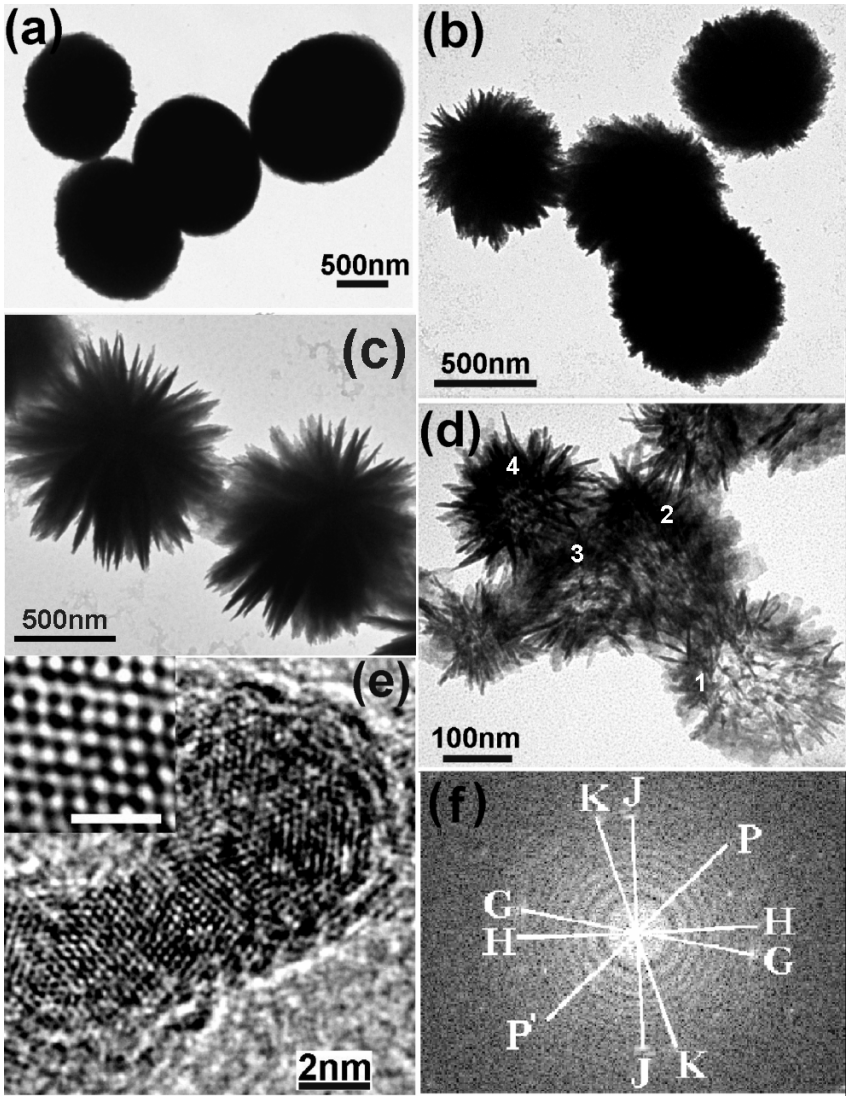

Figure 5.4 (a) Nanospheres with rounded edges (synthesis conditions: laser power 50 mJ, ablation time 2 h, 35% ammonia solution, drying in air). (b-c) Nanoflowers with numerous protruding spiky surfaces (synthesis conditions: laser power 100 mJ, ablation time 8 h, 35% ammonia solution, drying in air). (d) Hollow-flowers with tunnels connecting from the centre to the outward shell (synthesis conditions: laser power 100 mJ, ablation time 10 h, 35% ammonia solution, drying in a sealed tube). The numbers denote the individual hollow-flower. (e) HR-TEM image of a single NR, the inset shows the atomic arrangement and scale bar 1 nm. (f) The Fourier-Filtered Transform (FFT) pattern corresponding to the region shown in (e). K, J, H, G, P and P' label the positions of the six domains (see text for details).

Compared to the flower-like structures, the hollow-flowers are less common. A longer drying time in an above ambient temperature aids the small crystallites to move freely in the solution enabling oriented aggregation. The ratios of population among the nanosphere, nanoflower and hollow-flower structures are approximately 30%, 60%, and 10%, respectively (based on a total of 800 TEM images), noting that the statistical ratios vary for different experimental conditions. In general, a higher synthetic energy (*i.e*. high laser power, long ablation time, high ammonia concentration and long drying time) leads to better crystallinity, but larger size for the products.

In principle, assembly is energetically favoured because the formation of larger crystals can greatly reduce the interfacial energy of isolated NPs or NRs. Therefore, most of our final products are either well-defined leaf-like structures (see Chapter 4) or self-assembled flower-like architectures if the TEM grid dried naturally in air. Only occasionally were monodispersed NPs or isolated NRs seen by TEM. The mechanism for how these lower dimensional building blocks construct to higher dimensional arrangements, rather than random clumps, is still unclear. However, the above evidence indicates that 'oriented attachment' [37] was observed among the crystallites, in which a larger crystal structure is formed from smaller ones by direct joining of suitable crystal planes. In particular, in the HRTEM image of Figure 5.4(e) taken from a single NR, the periodic lattices show the atomic arrangement (Figure 5.4(e), inset) with very few defects, and reflect the relationship between the orientation of the NPs and the crystallography of the ordered NR array. The corresponding Fourier-Filtered Transform (FFT) pattern illustrates that the nanocrystal consists of six domains with sixfold twins. The split spots K and J, H and G in the FFT pattern is due to the small angle between the twin boundaries. The reflections P and P' in Figure 5.4(f) are not split, and represent the coherent positions of the twin boundaries.

Information regarding the chemical bonding structure was obtained from Fourier transform infrared spectroscopy (FTIR). Figure 5.5 shows the FTIR spectra of the above-mentioned different morphology of carbon nitride crystals, which exhibits several peaks related to the chemical bonding between carbon and nitrogen [38]. The region 1000-1500 cm^{-1} corresponds to C-N single bonding, while the

regions 1500-1750 cm^{-1} and 2150-2300 cm^{-1} are related to C=N and C≡N bonding, respectively. Similar spectra were also obtained by Zimmerman and co-workers [39]. In our case, for the nanosphere structures (Figure 5.5(a)) the two peaks at 1040 cm^{-1} and 1406 cm^{-1} correspond to the C-N stretching mode. The absorption band at 1639 cm^{-1} is assigned to the stretching vibrational modes of C=N. Moreover, a small peak at 2208 cm^{-1} can probably be attributed to C≡N bonds, although it is much weaker compared with the other stretching modes. A broad band centred at 3464 cm^{-1} is due to NH group vibrations [40]. The 558 cm^{-1} peak can be assigned to the out-of-plane bending mode for graphite-like sp^2 domains, which become IR active due to nitrogen incorporation into the bonding network. The obvious differences between these samples are that the intensities of all the features are weaker and broader for the nanoflower and hollow-flower shape nanostructures. We attributed this to the voids in the nanoflowers and the internal nanospaces existing in the hollow-flowers.

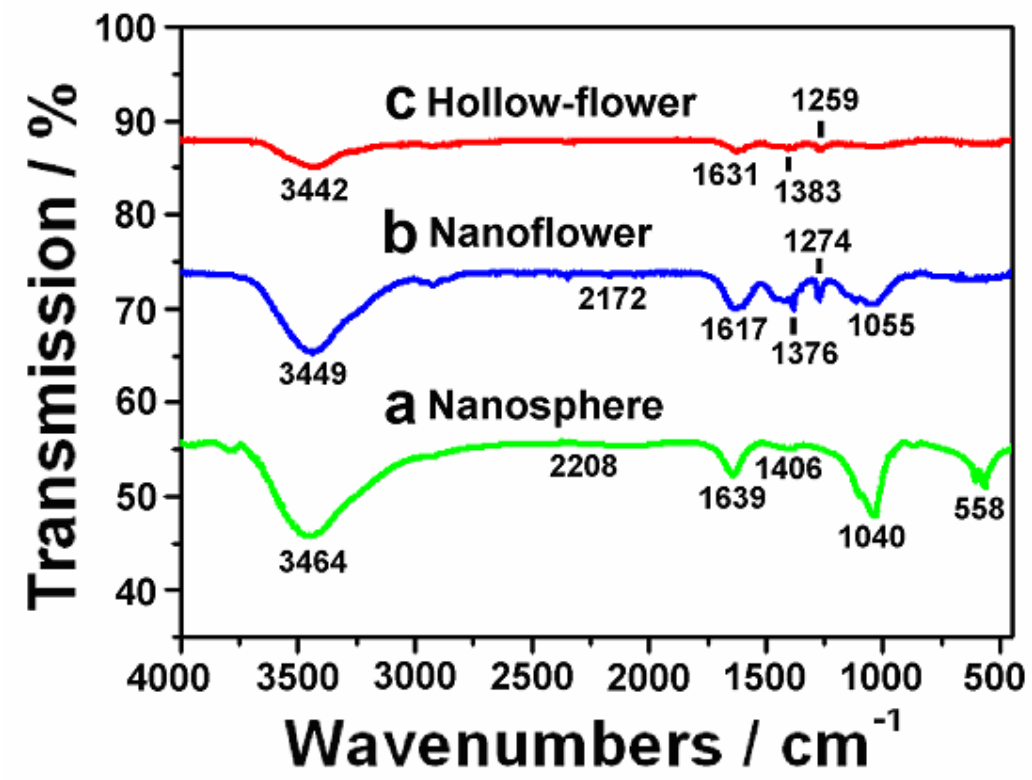

Figure 5.5 FTIR spectra of three different carbon nitride structures: (a) nanosphere, (b) nanoflower, (c) hollow-flower.

§ 5.2.2 Control of the quality of self-assembly

§ 5.2.2.1 Diffusion of the building blocks

Usually, ordered organization was obtained following evaporation of a drop of a nanocrystal solution that had been deposited onto a TEM grid. Figure 5.6(a) shows a typical symmetric carbon nitride 'flower' together with its nano-petal building blocks (which look like flattened rods in the TEM). Figure 5.6(b) shows that these nano-petals appear fused together and 'interwoven' to form a lattice-like framework of the flower-like superstructure. The figure also shows the NPs that surround each nano-petal, and which fill in the holes within the framework to produce a dense, solid structure. Energy-dispersive X-ray (EDX) analysis confirms that carbon and nitrogen are present in all these structures, and micro-diffraction pattern (MDP, Figure 5.6(c)) was also consistent with crystalline hexagonal β-phase carbon nitride oriented along the [001] zone-axis. Several [001] patterns in Figure 5.6(c) can be identified at the same time, indicating that the nano-petals consist of several domains, with different rotational orientations contributing to the diffraction pattern. The HR-TEM image in Figure 5.6(d) shows that the nano-petals at the very edge of the flower contain very few defects and are single crystalline, as was anticipated from the MDP. Again, the lattice fringes (d_{200} = 0.28 nm, $d_{1\bar{4}0}$ = 0.15 nm) and their angles (106°) are in good agreement with the calculated values for hexagonal β-C_3N_4 [41].

The smaller NPs, which lie in and around the nano-petal-framework comprising the flowers, appeared to be mobile with respect to this framework, and diffused outward from the centre of the flower with longer drying times. The results of this diffusion can be seen in Figure 5.6(e), where the solid carbon nitride flower (similar to that in Figure 5.6(a)) has become hollow. The NPs have diffused from the centre but remain loosely attached to the outside, making the outer shell of the flower appear fuzzy. The thickness of the fuzzy shell was ~ 140 nm and that of the hollow core was ~ 200 nm (shown as a lighter colour in the image). When the suspension was placed onto a hot-plate at 200ºC for 0.5 h, the hollowing process was accelerated to form a semi-core-shell structure. The radial distribution of the NRs formed

channels leading from the centre to the shell (Figure 5.6(f)). Another type of hollow structure was observed when the core-shell structures were essentially separated by a hollow tunnel, without linkage to the sphere (Figure 5.6(g)).

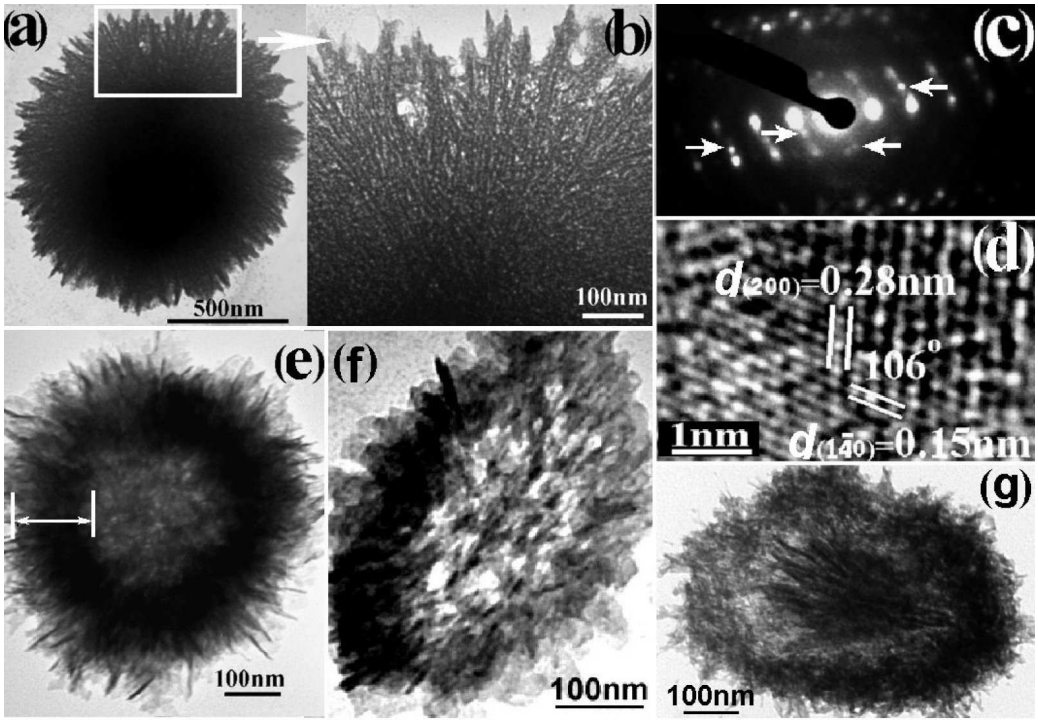

Figure 5.6 TEM image of the flower-like structures produced by LP-PLA of a graphite target in 35% ammonia solution (laser fluence 125 mJ/pulse) for 5 h. (b) A higher magnification image of the framed region in (a), showing a high density of NPs surrounding the nano-petal framework. (c) [001] zone-axis MDP from the tips of the nano-petals in (b), which corresponds closely to the calculated interlayer *d*-spacing of β-C_3N_4. Arrows point to different sets of [001] reflections (see text). (d) HR-TEM image recorded from the edge of the flower nanostructure that is oriented along [001]. (e) TEM image of a hollow flower formed after 8 h LP-PLA and prolonged drying. (f) Semi core-shell structure. (g) core-shell structure with a hollow tunnel.

§ 5.2.2.2 Interconnection between the big structures

Self-assembly normally occurs when nanoscale objects interact with one another through a balance of attractive and repulsive interactions. If the attractive force is dominant, the components may interconnect and form larger aggregates. In contrast, the exterior appearance of the interlinked nanostructures did not change appreciably when the interaction was weak. It was found that the interconnections among the structures were different. Figure 5.7 shows two examples of these cluster-like combinations, for nanospheres and nanoflowers. Figure 5.7(a) shows a single typical nanosphere with a dense surface, similar to those mentioned previously in Figure 5.4(a). Figure 5.7(b-c) shows that two neighbouring spheres can be fused together, or just joined loosely via their outside edges, with no change of internal structure. However, for the nanoflowers, the situation was different. Figure 5.7(e) shows that when two nanoflowers fuse, the inner spaces between the NRs were integrated throughout the entire cluster structure. One important note is that the fusing together of pristine nanoflowers alters the crystalline size slightly (~800 nm in diameter) but the morphology of nanoflower remained (Figure 5.7(f)).

If the TEM grid was replaced by a silicon substrate, and the previously prepared carbon nitride seed solution was applied and dried naturally in air, similar morphologies to those shown in Figure 5.7 were obtained. However, the nanospheres were now formed with a more uniform size distribution, as shown in Figure 5.8(a-b). Some nanospheres (size about 500 nm-1 μm) were attached with a boundary visible in between (highlighted by arrows for clarity), as shown in Figure 5.7(b-c). The interaction between such interconnected nanospheres is weak since they could be broken up with a few minutes' of sonication. In contrast, the nanoflowers were dispersed individually (Figure 5.8(c)) with a larger size distribution (~1-15 μm). It is noted that the size of the nanoflowers found by SEM on the Si substrate appeared much larger than those under TEM observation (size about 500 nm-800 nm). This is probably due to some of the nanoflowers fusing together completely to produce larger, interlinked nanoflowers (see Figure 5.8(d), highlighted by the arrow). Such nanoflowers are stable and sustainable without any change even after a few hours' of sonication. The reason the nanoflowers fused

more completely was to do with the different interaction between the particles within the seed solution and the two types of substrate. The TEM grid was normally placed onto a filter paper and a drop of carbon nitride aqueous solution was pipetted onto the grid. Due to the presence of the filter paper, water was quickly removed. For the SEM sample on a Si substrate, the droplet of solution took at least 2 h to dry in air. This allowed sufficient time for the nanoflowers to aggregate. Further investigation needs to be carried out.

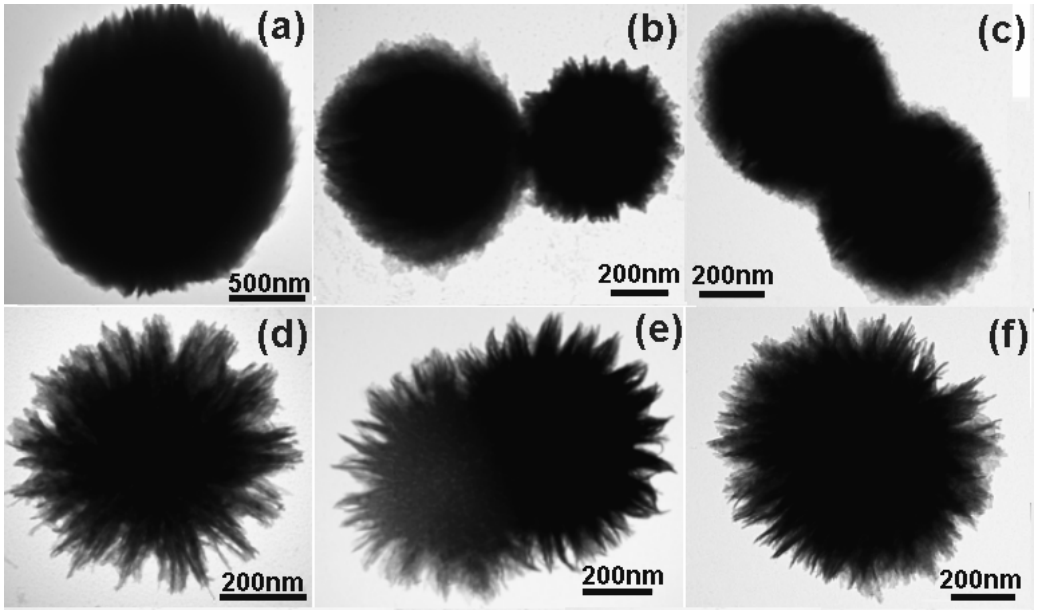

Figure 5.7 Examples of coalescence (eventually leading to clustering) of dense carbon nitride nanospheres and porous nanoflowers. (a) A single nanosphere, (b) 2 nanospheres touching, (c) 2 nanospheres fused together. (d) A single nanoflower, (e) 2 nanoflowers partially fused together, (f) 2 nanoflowers completely fused.

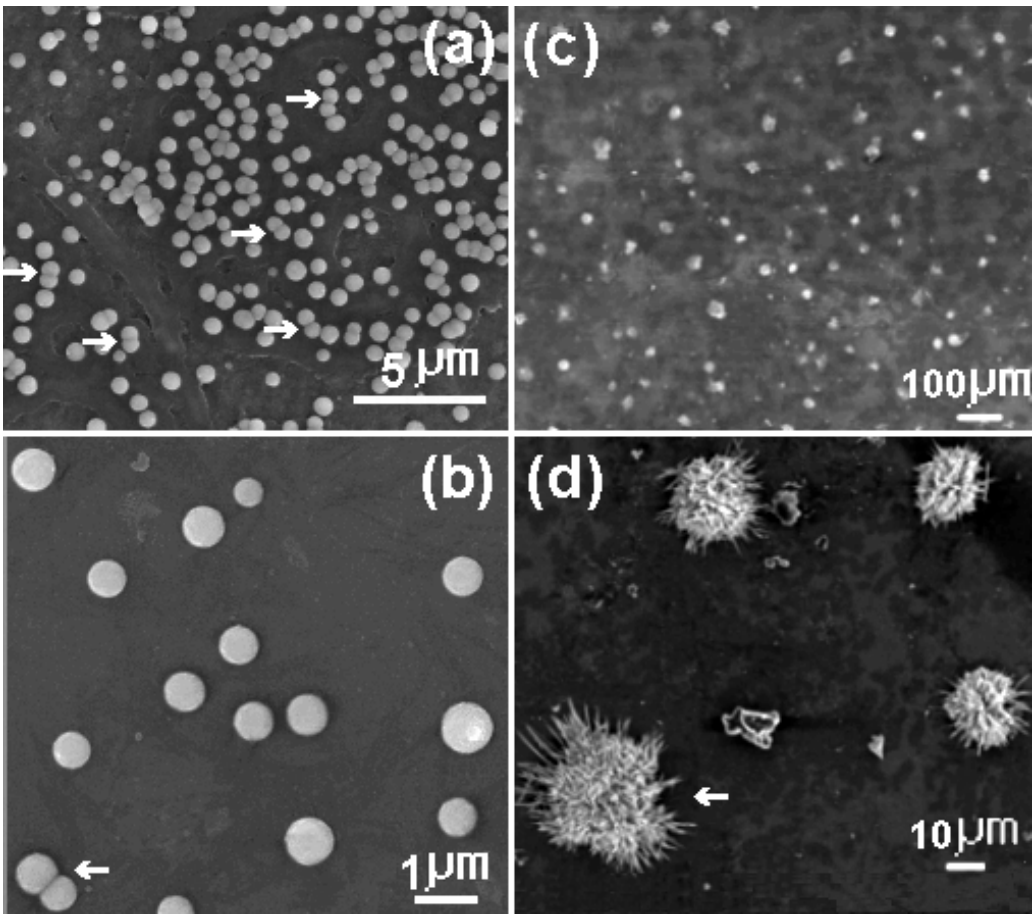

Figure 5.8 (a-b) nanospheres (carbon nitride seed solution is identical to that used for Figure 5.4(a)). The fused nanospheres are marked by arrows. (c-d) nanoflowers (carbon nitride seed solution is identical to Figure 5.4(b-c)). The drying process was in air. The arrow in (d) shows possible fused nanoflowers. Note that image (b) and (d) are recorded in higher magnification from (a) and (c), respectively.

Control experiments provide some evidence to support this proposed mechanism. Under identical conditions, a droplet of carbon nitride solution was deposited onto a Si substrate and placed into a sealed tube. The drying process was now estimated to be around 8 h. As expected, larger flowers constructed from hundreds of thin plates were formed (Figure 5.9(a)). Careful observation found that these larger flowers were actually an aggregate of more than one nanoflower. The boundary between the nanoflowers was perfectly fused and aligned. The enlarged

region in Figure 5.9(a) marked by black box shows that numerous nanoplates are bunched up and cross-linked with recognizable boundaries or voids between the component subunits (Figure 5.9(b)), which are still maintaining their close proximity. Such results can be further seen in Figure 5.9(c-d). Occasionally, flowers were not fully developed, since the rate of aggregation among the nanoflowers varies depending upon local conditions. But the arrows marked in Figure 5.9(c-d) clearly indicate the fusion of the adjacent nanoplates. Given sufficient time (*e.g.* by prolonging the drying time), the growth of the flower will fully complete into three dimensions.

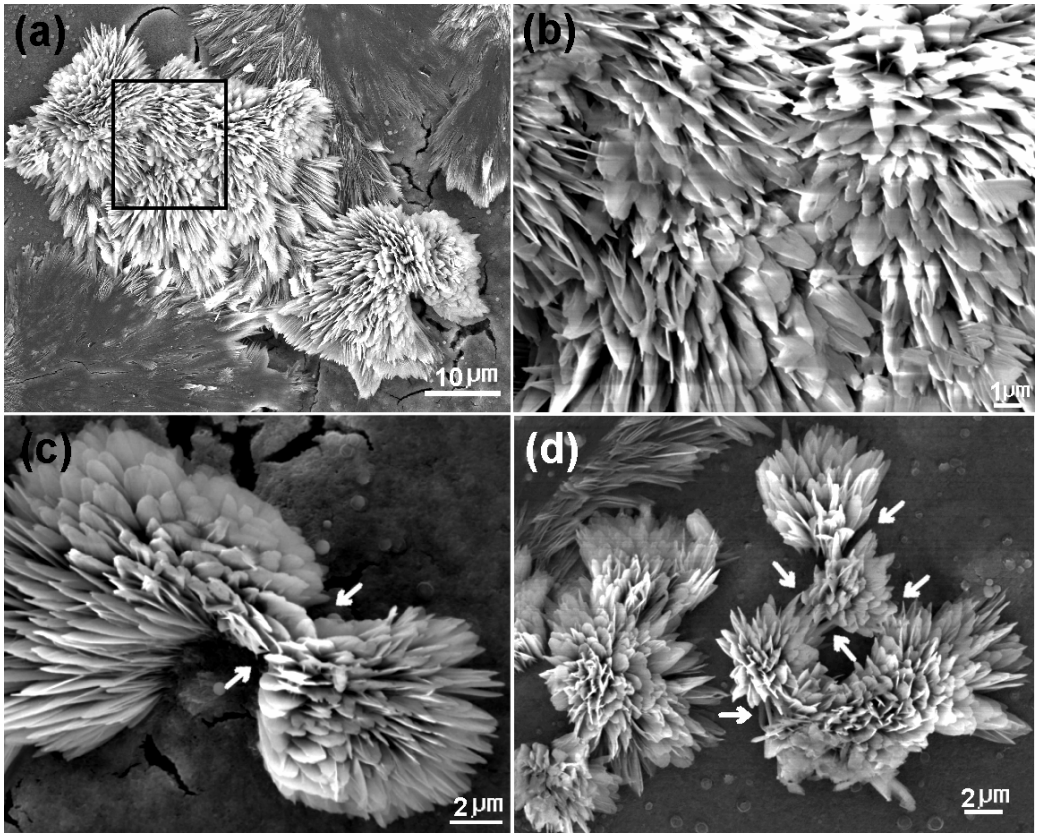

Figure 5.9 Fused-flower (carbon nitride seed solution is identical to that used in Figure 5.4(b-c)). Drying process is in a sealed tube (~ 8 h evaporation). See text for discussion. Arrows in (c) and (d) are marked for clarity.

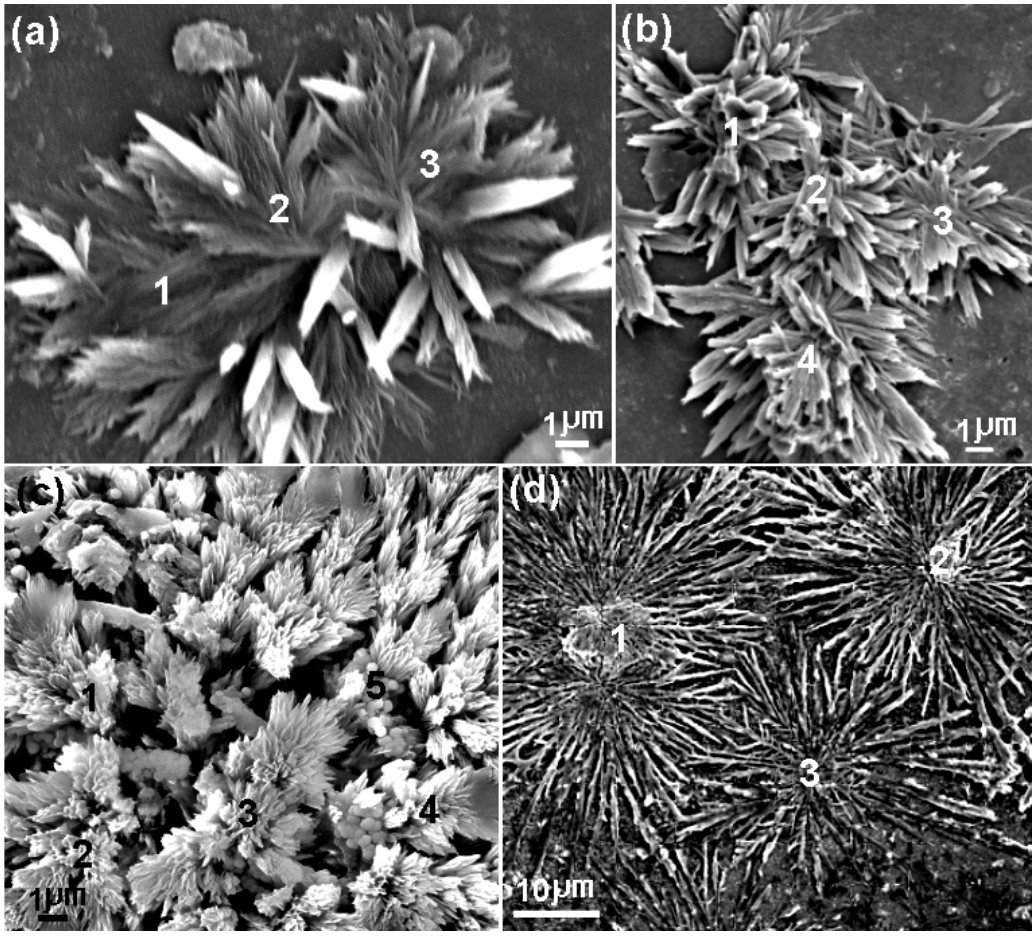

Figure 5.10 (a-b) 3D interconnected flowers. (c-d) 2D flattened flowers (synthesis conditions: 35% ammonia solution, laser power 100 mJ, 3 h ablation and dried in a sealed tube, (c-d) seed solution was diluted by using deionised water). Numbers in (a-d) denote the individual flower.

A few more examples of interconnection between larger complex structures are given in Figure 5.10. As shown in Figure 5.10(a), the neighboring long petalled crystals can further expand themselves and eventually merge into an interconnected structure [42]. At least 10 petals are needed to form the secondary flower-like architectures. Some of them sprouted out to three dimensions but some were lying down along the substrate (see 3rd flower in Figure 5.10(b)). However, when using diluted carbon nitride seed solution, morphology changes (Figure 5.10(c-d)) in the mesoscopic structure may be correlated to interactions between nanocrystals. The

interconnection between those flowers was also observed, although the forces seemed weaker (larger voids exist, see the numbered regions in Figure 5.10(c-d) for demonstration) compared with those shown in Figure 5.9. The disappearance of the 3D structural dimension and the occurrence of 2D flattened flowers which cover the substrate are believed to be a result of a significant decrease in the interaction between the dispersed nanocrystals in the droplets. In a slow evaporation, the attractive force between NPs is low and they are likely to diffuse close to the substrate leading to formation of 2D flattened structures.

§ 5.2.3 Dynamic study of self-assembly formation

§ 5.2.3.1 Influence of the drying time

Morphology development of the high-order grass-like architectures at different growth stages was monitored by SEM (Figure 5.11). The evaporation rate is controlled by either the substrate temperature or the solvent saturation degree of the surrounding atmosphere. The seed solution used was spherical NPs with an average particle size of 15-20 nm under TEM observation, previously discussed in Chapter 4 (see Figure 4.11(a)). When the droplet of carbon nitride NPs solution was deposited onto a silicon substrate and placed on a hotplate, the solution dried quickly (about 30 min). In this case, the NP morphology remained, and small islands of NP aggregates dispersed on the surface sparsely (Figure 5.11(a)). In contast, if the droplet on the Si substrate was dried naturally in air (~2 h), 1D NR nuclei started branching on the surface and gradually formed 2D 'roots' (~200 nm in size), see Figure 5.11(b). If instead, the droplet was dried in a sealed tube (~8 h), the number of nanopetals increased and started interconnecting or aggregating (see the left side of Figure 5.11(c). The 2D primary nanopetals took about 12 h to coalesce into grass-like structures (Figure 5.11(d)). Upon further increasing the drying time to 24 h, the NPs adjusted their position and continued to assemble, stem-like, and eventually expanded into fully-developed 3D architectures (Figure 5.11(e)). In the enlarged image of Figure 5.11(f), it can be seen that nanopetals on each side stem were nearly

parallel to one another. Moreover, NR bundles can be clearly observed in each nanopetal (see the highlighted area in Figure 5.11(f)). It should be noted that such heterogeneous nucleation and growth in solution were not observed by means of TEM.

Similar experiments were also performed using the carbon nitride seed solution mentioned in Figure 4.16(a) (see Chapter 4). The starting seeds morphology was more complex than NPs used in previous time evolution study. Since it was observed that a flower exhibited a surface composed of NRs, we expect that a similar morphology should appear on Si substrate. However, no regular objects were detected by SEM when the droplet was dried in air. Only some low contrast flower-shape patterns (Figure 5.12(a)) were seen, which appeared uniformly dispersed. The enlarged image in Figure 5.12(b) shows that such patterns are actually formed by a number of particles with preferential arrangements, which were presumably the later nucleation sites for the growth of the flower. With controlled drying time (~8 h) in a sealed tube, large numbers of flower-like structures (Figure 5.12(c)) about 500 nm in size were distributed on the silicon surface. The enlarged image Figure 5.12(d) from the area of Figure 5.12(c) shows these nano-objects possess external bonding capacity or 'adhesiveness' for self-assembly and self-alignment. For example, they have extending 'arms' (NRs or nanopetals) ideal for external connectivity (highlighted by arrows in Figure 5.12(d)). Fully complex geometric flowers took more than one day to develop (Figure 5.12(e)). Such structures comprise numerous 1D NRs or 2D nanopetals with their long-axis pointing toward the centre of the flower. Those components were arranged side-by-side and some were tightly bonded each other (highlighted by arrows in Figure 5.12(f)).

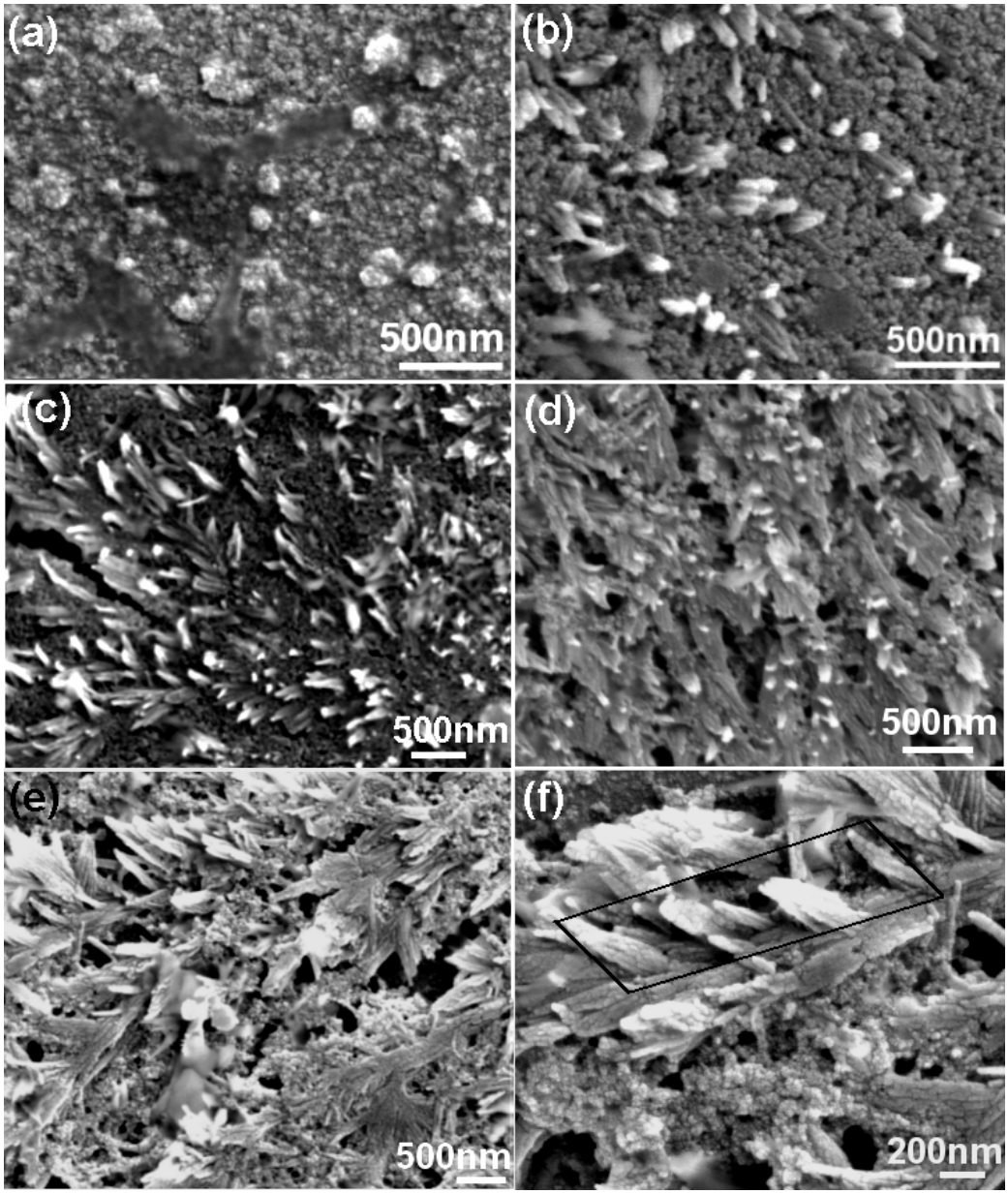

Figure 5.11 Time-dependent evolution of grass-like crystal morphology at different growth stages for (a) 30 min, (b) 2 h, (c) 8 h, (d) 12 h, and (e-f) 24 h, respectively. The box in (f) was marked for clarity of nanopetals arrangement. (Synthesis conditions: 35% ammonia solution, laser power 75 mJ, 10 min ablation, spherical NPs with an average particle size of 15-20 nm were used as seeds, as shown in Figure 4.11(a). See text for discussion).

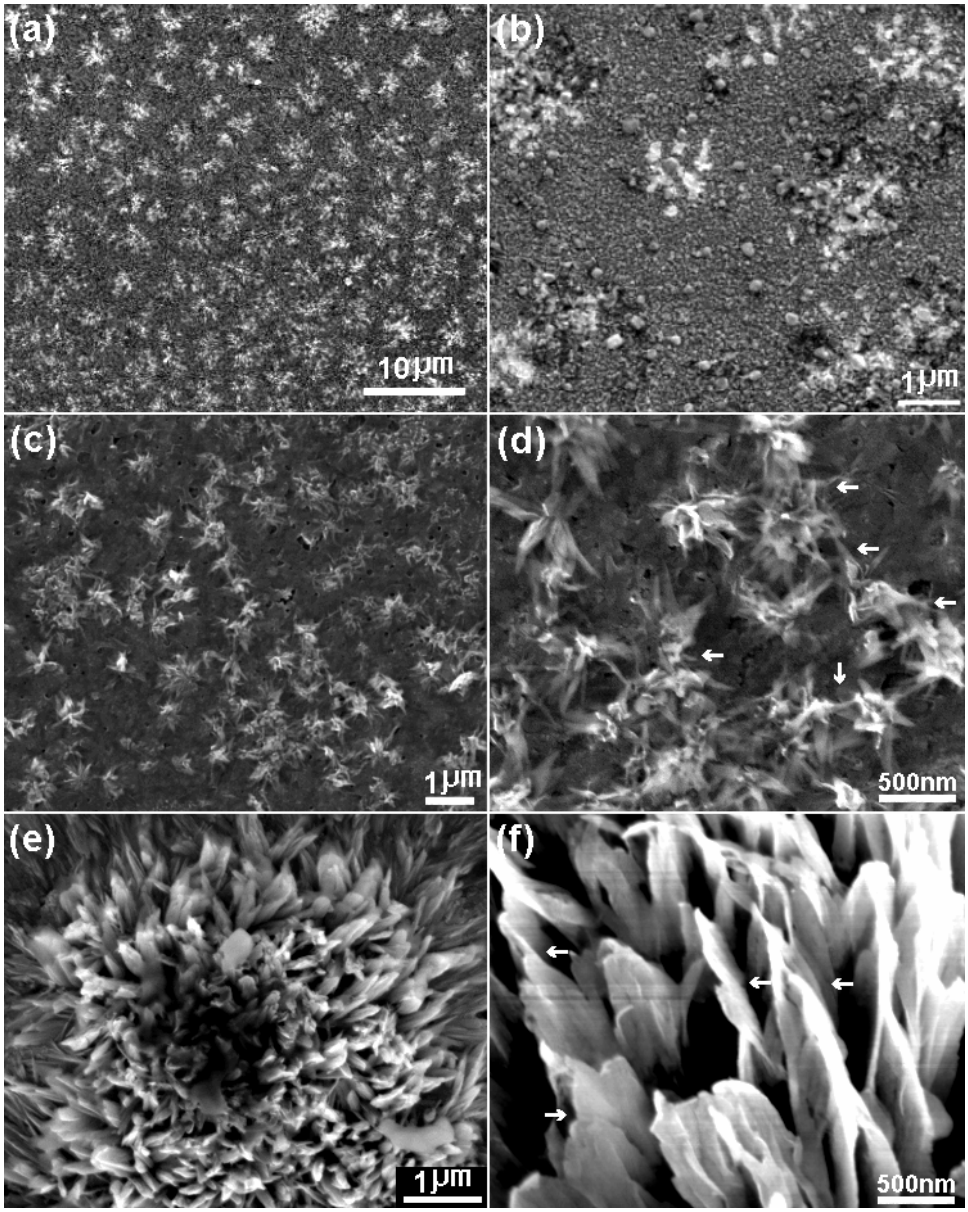

Figure 5.12 Time-dependent evolution of the flower-like crystal morphology at different growth stages for (a-b) 2 h, (c-d) 8 h and (e-f) 24 h, respectively. Arrows in (d) and (f) are marked for clarity of bonding components. Note that images (b), (d) and (f) are recorded at higher magnification from (a), (c) and (e), respectively. (Synthesis conditions: 35% ammonia solution, laser power 50 mJ, 12 h ablation, a flower exhibited a surface composed of NRs, where the NRs radiate outward from the centre as shown in Figure 4.16(a). See text for discussion).

From the above discussion, it seems that the morphology of the initial stage of complex architectures (grass-like or flower like) was a small aggregate of compacted 15-20 nm-sized dense particles, which were approximately spherical in shape. Although the nucleation and growth of grass-like or flower-like carbon nitride superstructures might accompany NP fusion and self-alignment to bigger building blocks (such as NRs or nanopetals), no direct evidence was observed for this direct aggregation. Fusion and self-organization may also be associated with thermal motion of the droplets, for example, the evaporation speed, which is determined by the temperature and the amount of air flux. However, what is the driving force that controls the final hierarchical complex? The mechanism is still not fully understood. One possibility is that growth continues within the local fluid environment as long as there is substantial mobility of the seed particles for further exchange. If the process is sufficiently slow, this will continue until all the building blocks adjust to their desired (lowest energy) position. Evidence for this is that the fully developed grass-like or flower-like complexity was only observed on a decreasing the evaporating rate, *i.e.* for drying times above 12 h in the later growth stage (Figure 5.11(e-f) and Figure 5.12(c-d)).

§ 5.2.3.2 Influence of the starting seed solution

The starting seed solution can strongly influence the 2D and 3D arrangements of the nanostructures. As expected, when leaf-like structures were present in the seed solution, these aggregated to form 3D nanoleaf clusters (Figure 5.13(a-b)). When the concentration of the carbon nitride seed solution was increased by dropping more than one droplet onto the substrate, the organization occurred on larger scale (Figure 5.13(c)). The 3D arrays were very inhomogeneous in size and shape with NPs dispersed on the surface of the nanoleaves. This result is obtained whatever the nature of the nanocrystals. When using the seed solution identical to that in Figure 5.4(a), i.e. the nanospheres with rounded edges, increasing the particle concentration also increases the size and density of the resulting clusters (Figure 5.13(d)). Some of the nanocrystals have elongated along the long-axis and lost their spherical shape (see the numbered clusters in Figure 5.13(d)), but show particular

orientation. In this case, the concentration gradient appearing during the evaporation favoured a convective flux. The solution contained much more dispersed nanocrystals, which increased the chance to aggregate and the interaction between the particles [43].

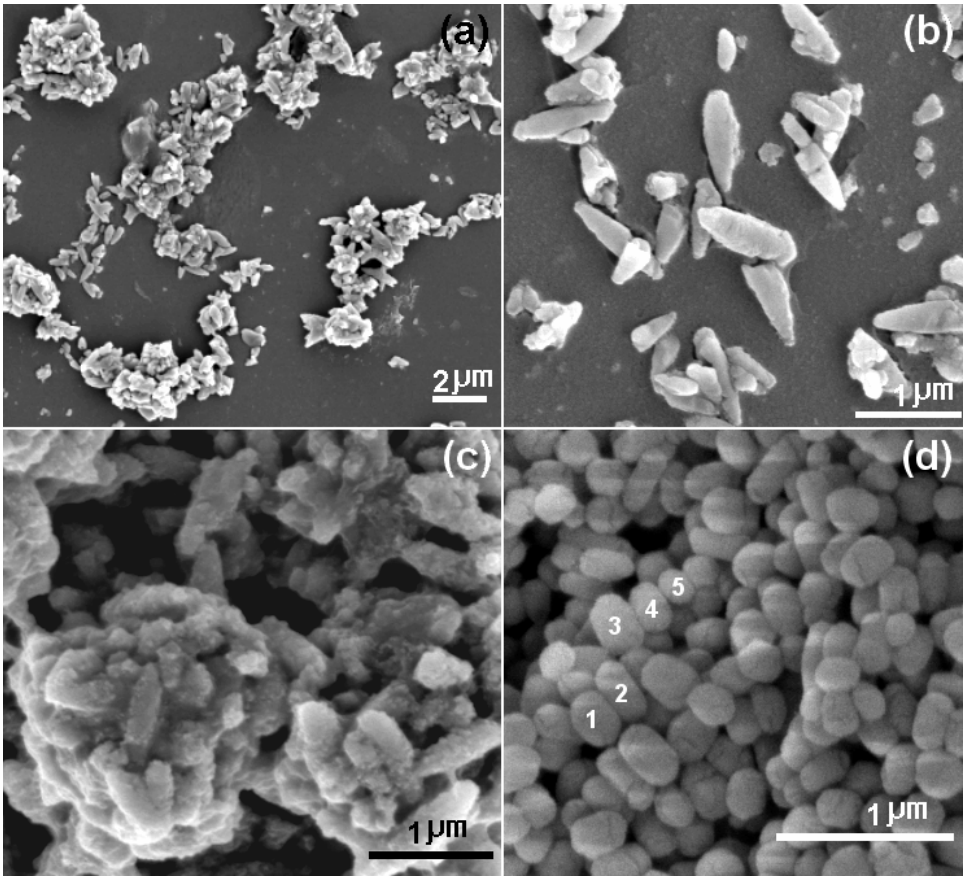

Figure 5.13 SEM images of different leaf-like clusters obtained by drying the carbon nitride colloidal solution in air. (a-b) Sparse, small clusters formed using one droplet of solution (synthesis conditions: laser fluence of 100 mJ per shot, 35% ammonia solution 7 h for ablation time). TEM image shows uniform leaf-like structures with average length about 400 nm, see Figure 4.13(d). Note that image (b) is recorded in higher magnification from part of (a). (c) Larger, denser clusters formed when more than one droplet was deposited on the substrate. (d) Clusters formed when using the seed solution identical to that in Figure 5.4(a). Individual clusters in (d) are numbered for clarity.

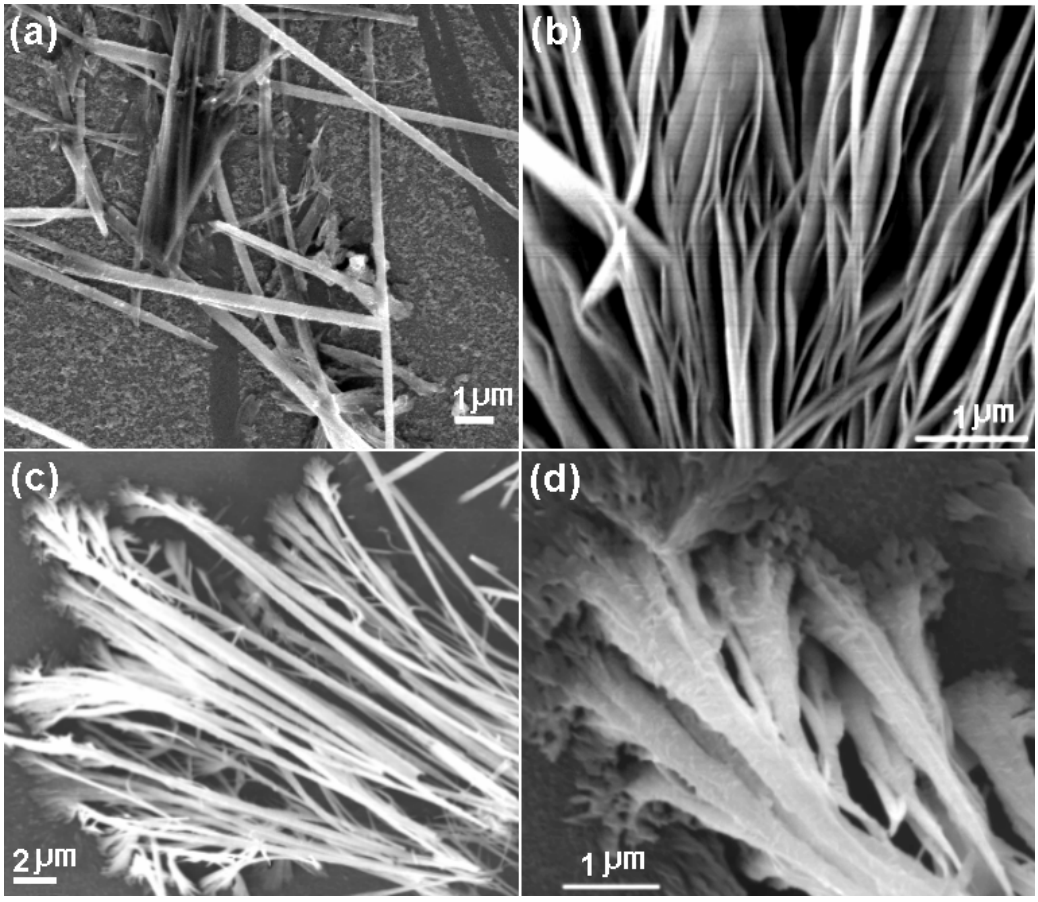

Figure 5.14 SEM images of different rod-like patterns obtained by drying the carbon nitride colloidal solution (a) in air (synthesis conditions: 25% ammonia solution, 50 mJ/ pulse, t = 1 h, TEM image shows the isolated carbon nitride NRs (see Figure 4.17(a)). (b) in air and (c) in sealed tube (synthesis conditions: 25% ammonia solution, 50 mJ/ pulse, t = 3 h, TEM image shows branched NRs (Figure 4.17(b)). Image (d) is recorded at a different magnification to (c).

Further experiments were performed using the carbon nitride seed solution prepared in 25% ammonia solution. From the discussion in Chapter 4.2.2.3, we found most of the products were a sparse collection of isolated NRs or rod-like branches (Figure 4.17). Using these as seed solution and varying the concentration and solvent evaporation rate, rod nanocrystal formation was been observed with different morphologies (Figure 5.14). For example, irregular chaotic rods (Figure

5.14(a)), rods with branches (Figure 5.14(b)), and celery-like structure (Figure 5.14(c-d)). One thing these morphologies have in common is that they are all originally made from from rods shaped seed particles.

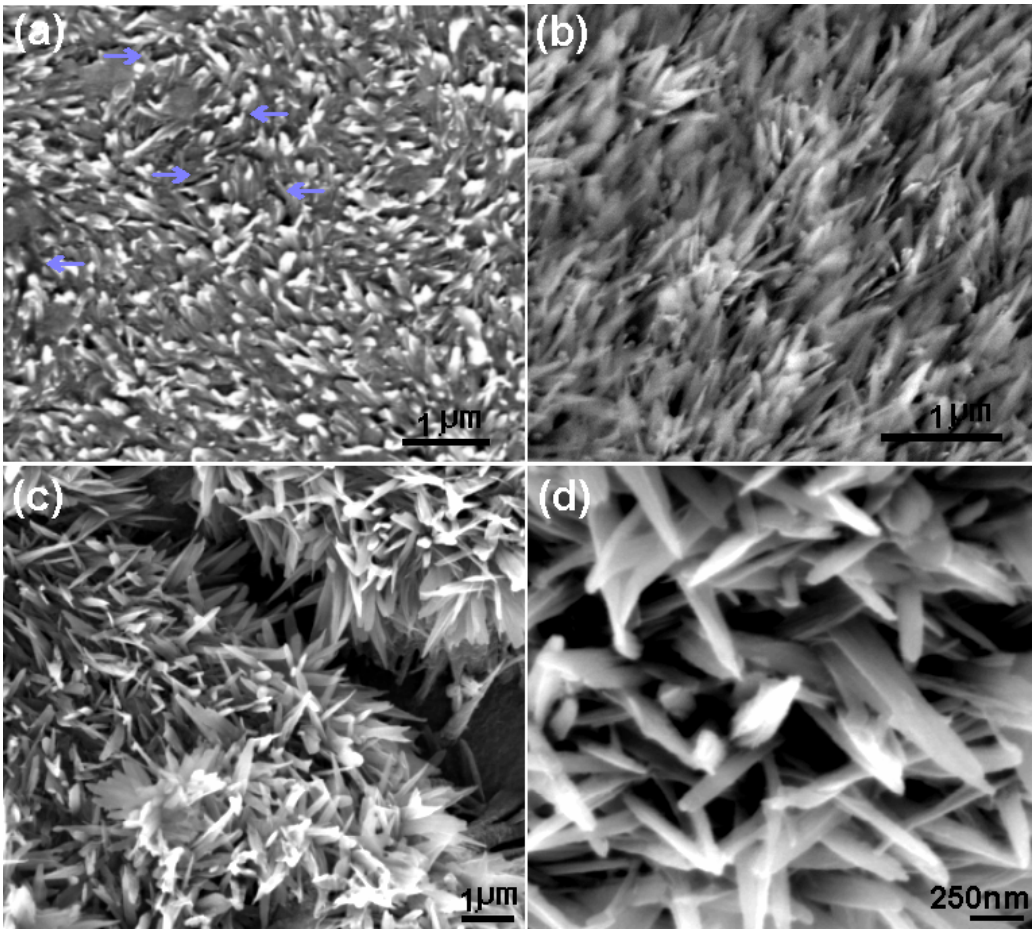

Figure 5.15 SEM images of carbon nitride 'grass-like' structures following ablation times (a) 0.5 h, (b-d) 2 h (synthesis conditions: laser power 125 mJ, 35% ammonia solution, and drying process: (a-b) drying in air and (c-d) drying in a sealed tube). Note that image (d) was recorded at high magnification than (c). Arrows in (a) point out the vacancies and cracks within the film.

It has been found that the size of the NPs in the initial starting solution is also very important in determining the morphology of the carbon nitride hierarchical nanostructures. If the starting seeds are short rods (Figure 5.15(a)), this would

favour the sticking of the NRs onto the substrate. The vacancies or cracks observed in Figure 5.15(a) are probably due to the fact that not enough nanocrystals were deposited on the substrate. However, if the seed solution contains sufficient number of nanocrystals with longer (about 500 nm) length, rod-rod interaction is dominant and they tend to form a denser and rougher grass-like surface (Figure 5.15(b)). The tips of those rods are very blurred, which implies that the solvent-substrate interaction becomes unstable. With longer drying time, an identical seed solution coated on the substrate formed an homogenous grass-like film (Figure 5.15(c)) with plenty of radial NRs (50-200 nm in width, 1-5 μm in length). It seems that in a slow evaporation process, increasing the size and the number of the NRs is beneficial to improve the crystallinity of the individual NRs and the uniformity of the film (Figure 5.15(d)).

The crystallinity improvement related to the atomic and nanocrystal ordering was further observed by TEM and HRTEM. Under the identical synthesis conditions, but using different drying methods, Figure 5.16(a) and (b) show apparent differences between those NRs subunits corresponding to Figure 5.15(b) and (c), respectively. When the solution is immediately dried in air (with the help of filter paper), the NRs were parallel-aligned and were 50-80 nm width and had a short length. The outline of the NRs was very blurred (Figure 5.16(a)). However, when drying was very slow, the NRs were very sharp, had longer length and larger width (~80-200 nm). Some NRs were overlapped and tilted away, similar to those shown in Figure 5.15(c-d). These results support the previous SEM observations.

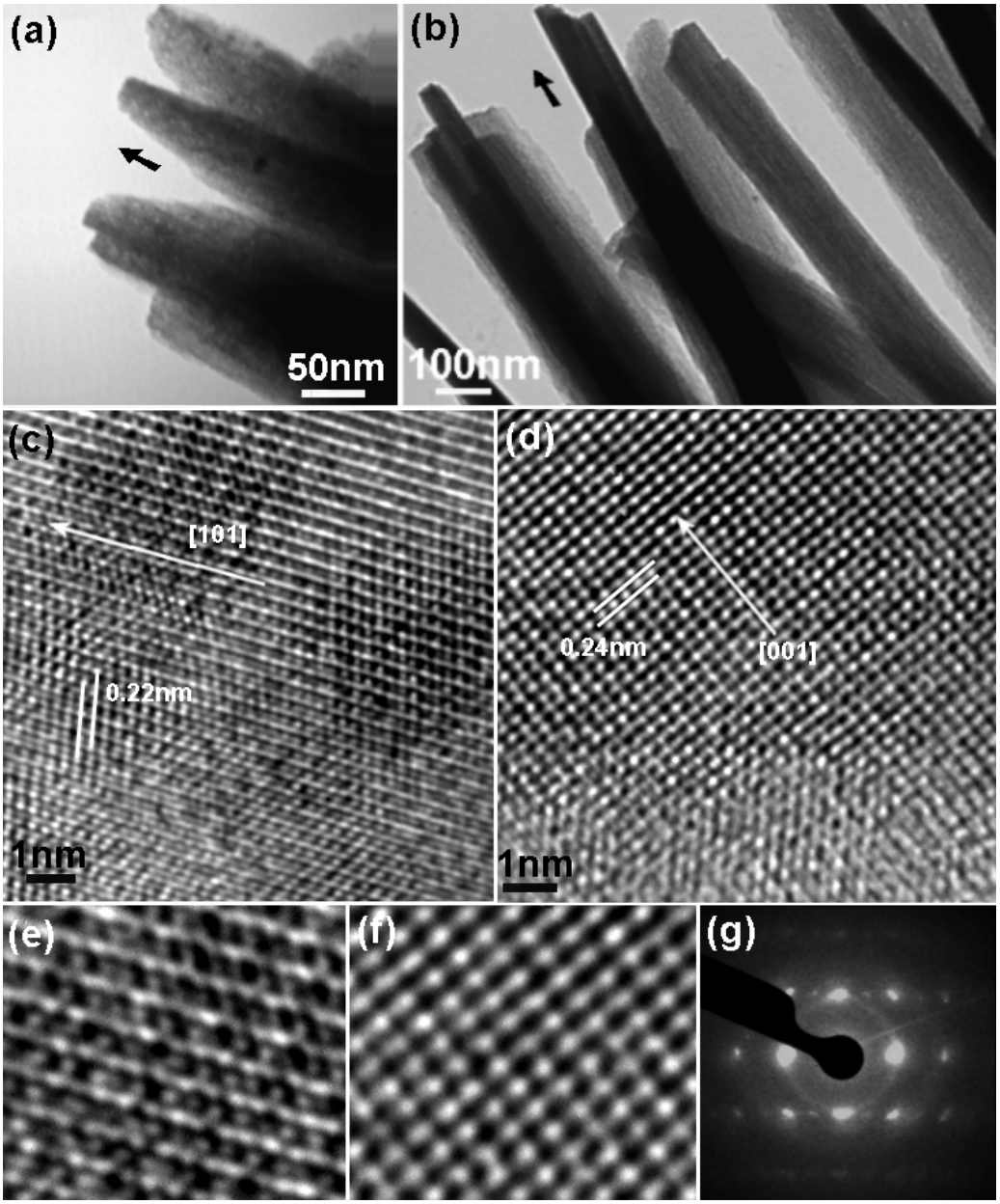

Figure 5.16 (a-b) TEM images of NR building blocks that form the 'grass-like' structures shown in Fig.5.15. (Synthesis conditions: laser power 125 mJ, 35% ammonia solution, 2 h ablation times, and drying process: (a) drying in air and (b) drying in a sealed tube). (c-f) HRTEM images recorded from the rods. (c) and (e) correspond to the region in (a), while (d) and (f) correspond to the region in (b). Arrows in (a-d) point to the growth direction of the NRs. (g) Microdiffraction pattern of corresponding (f) HRTEM image.

From the HRTEM images shown in Figure 5.16(c) and (d) (which correspond to the rod area in Figure 5.16(a) and (b)), it was found that the crystallinity within the domain was different. However, the growth direction for those rods perfectly matched the orientation that appeared in the TEM images (highlighted by arrow in Figure 5.16(a) and (b)). The enlarged images of Figure 5.16(e) and (f) show the individual atoms and their arrangements in this small region. Figure 5.16(e) consists of two slightly distorted layers, which are superimposed with respect to each other, and joined in the [101] direction. Consequently, the C_3N_4 groups deviate slightly from a planar arrangement. In contrast, Figure 5.16(f) is more close to the idealized β-C_3N_4 structure. The atoms are linked with one edge parallel to, and one edge perpendicular to, the (001) plane, with regular order [44]. The micro-diffraction pattern (Figure 5.16(g)) from the self-aligned NPs (Figure 5.16(f)) shows the single-crystal type [001] zone-axis pattern. Thus, the orientation order among the NPs in the assembly was further confirmed.

§ 5.3 Arrangement of components among the architectures

The emergence of a novel hierarchical and self-similar crystal-growth process in our system is very exciting. However, a few unsolved questions remain. How does this spontaneous formation process happen? What are the origins leading to the self-assembly of large objects with controlled morphology and ordering from nano- to meso-scale? To answer these, experiments were performed to try to understand the arrangement of components among the architectures. The assembly process of 3D hierarchical nanocrystals by repeated nucleation and growth is illustrated in Figure 5.17. By careful observation, it was found that the mesophase flower has a symmetrical structure (Figure 5.17(a)), consisting of numerous 2D radial nanopetals with radial growth from a central nucleus [45]. In addition, each nanopetal is constructed from many tiny nanocrystals or NR subunits (Figure 5.17(b)), as seen at the edge of the nanopetals (also, see the later discussion). Surprisingly, just as for the nanopetals mentioned earlier in Figure 5.6(b), these NRs also appeared to be 'interwoven' together into a similar lattice-like framework (Figure 5.17(c-d), shown

by the arrows). Interestingly, the NPs or NRs can self-assemble into a petal-like architecture along the *c*-axis direction.

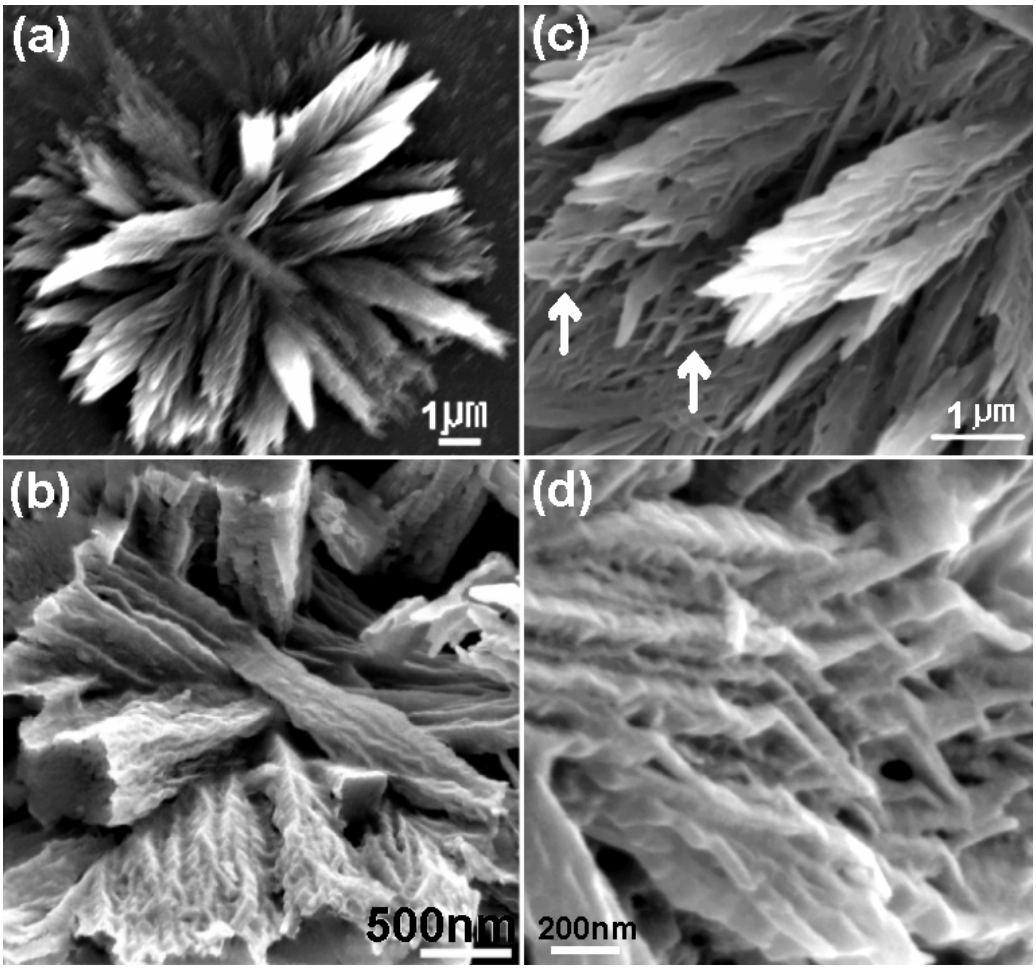

Figure 5.17 (a) An individual flower exhibiting multi-fold symmetry. (Synthesis conditions: 35% ammonia solution, laser power 100 mJ, 3 h ablation and dried in a sealed tube) (b-d) Different arrangements of components construct the final hierarchical superstructures. Arrows in (c) point to the 'interwoven' NRs framework.

The NPs attached side-by-side and fused into the wall of the nanopetal (Figure 5.18(a)). This has the effect of making the nanopetal surface rough and curved, and even made the two ends join together to form tubes (Figure 5.18(b)). Some nanopetals also revealed structures inside the tubes, see the highlighted arrows in

Figure 5.18(a-b) and (d). In some cases, they often terminated along a well-defined uniform growth edge with the flattened end (highlighted by arrows in Figure 5.18(c)). The inset of Figure 5.18(d) shows a primary subunit with size of about 20 nm. It is worth pointing out that the length of the nanopetals is in range of 1-20 μm, while the sizes of the subunit NPs have barely changed.

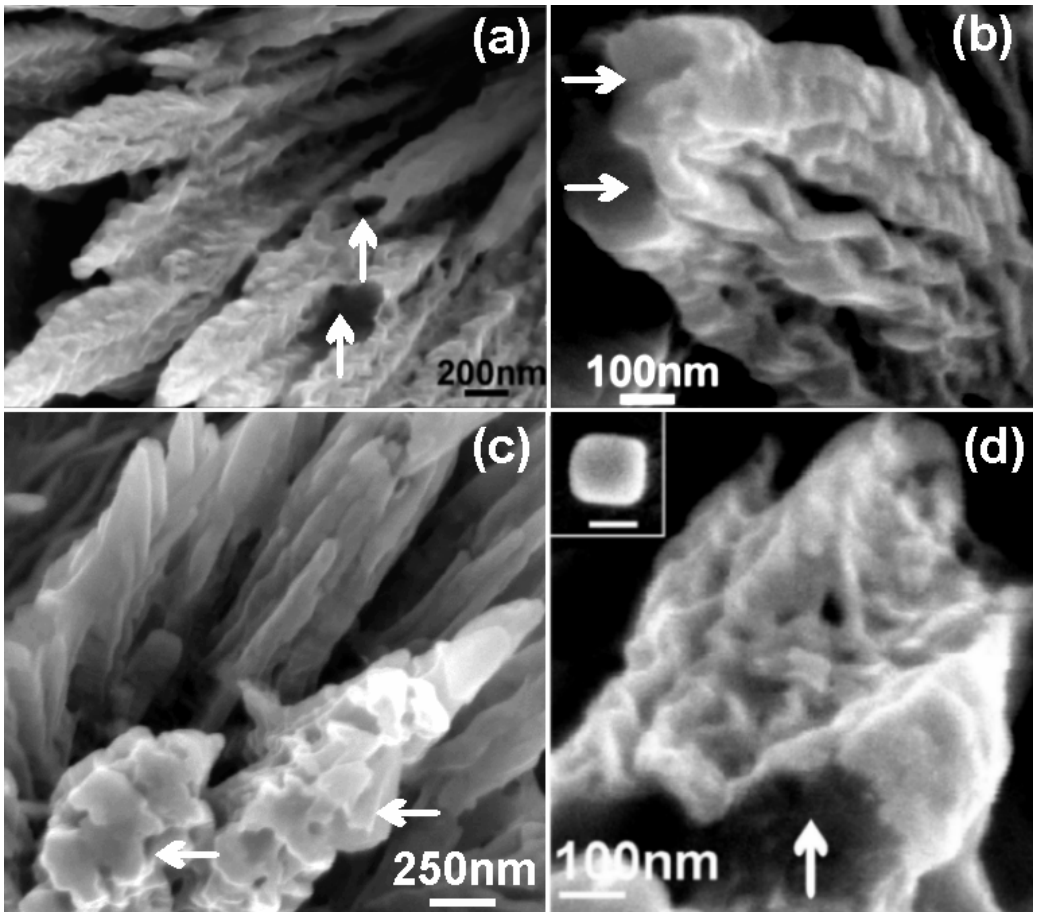

Figure 5.18 Nanopetal construction. Arrows in (a), (b) and (d) point to the inside surface of the tubular nanopetals. Flattened ends in (c) are highlighted by arrows. Inset of (d) shows a single nanocrystal as a building block, scale bar: 15 nm.

It seems that the solid Si substrate aids the initial self-assembly. That is, the presence of the substrate physically hinders growth in that direction; so many nanopetal branches are tilted away from the substrate. These structures are close-

packed but still have spaces between them. The excess vacancies between the nanocrystals are favourable sites to be filled up the continuous flux of particles, which is accomplished by consequently atom to atom lining up to reorganization and crystallization if the small building blocks are supplied continuously.

Figure 5.19 summarizes a possible process for the carbon nitride self-assembly, mentioned above. By the aid of the solid substrate, hierarchically ordered nanocrystals assemble towards the surface of the substrate. New nanocrystals nucleate on the existing crystals and share the same edges. These structures are close-packed but still have spaces between them. It is still unclear why the NPs or NRs form such arrangements rather than random clumps. Further investigation of this mechanism is required in the future.

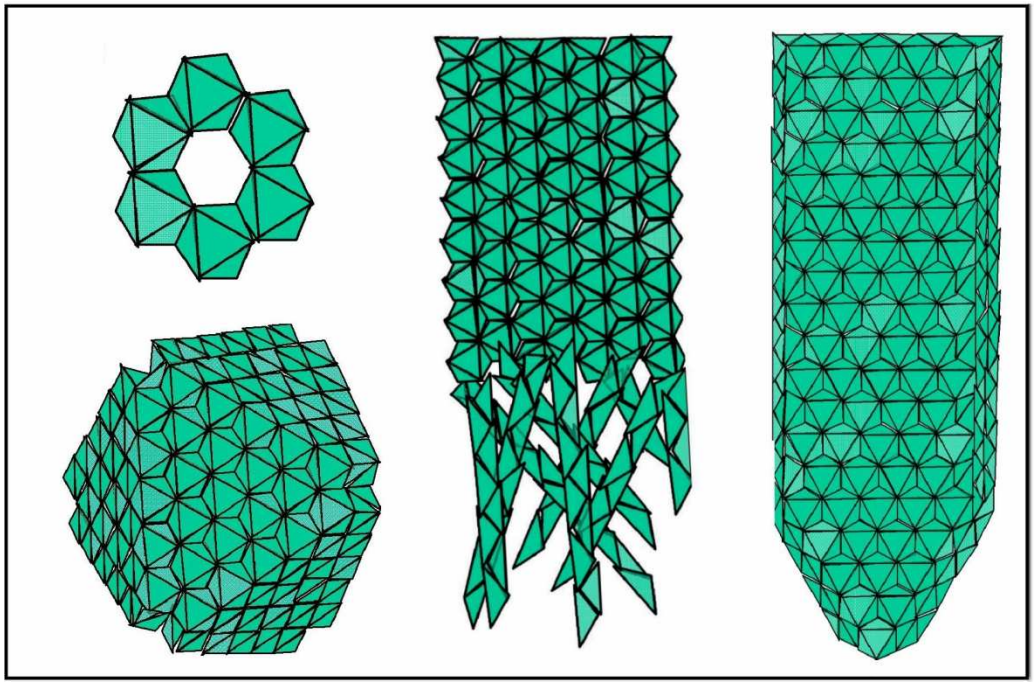

Figure 5.19 Schematic illustration of a suggested mechanism for the assembly of higher-order structures by nucleating new crystals through an edge sharing configuration.

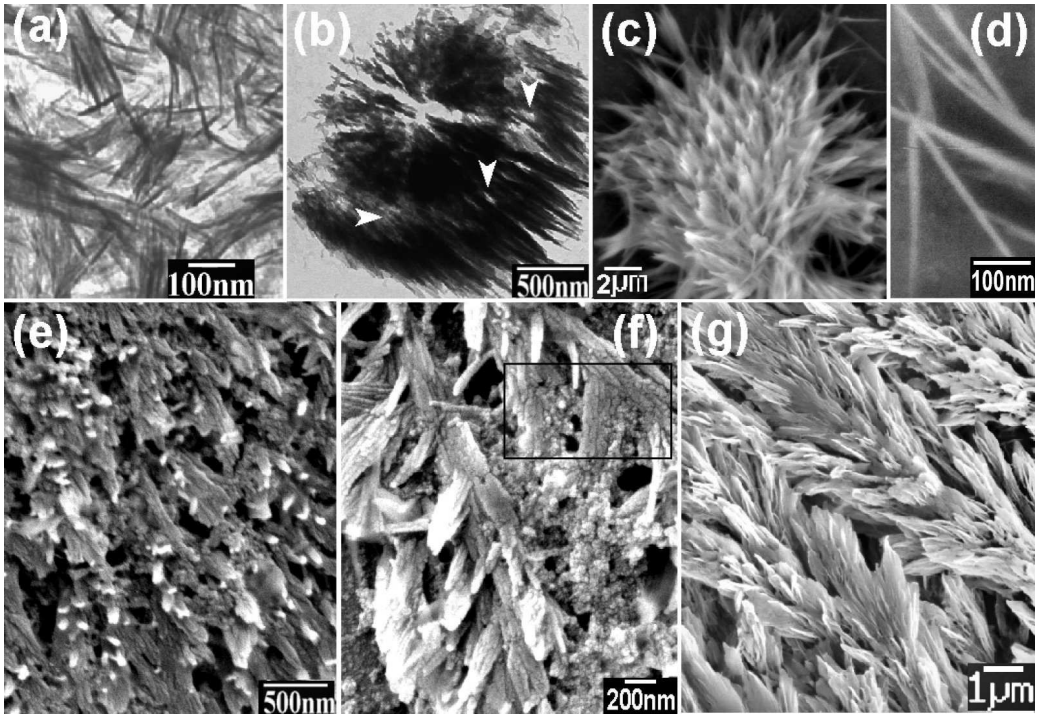

Figure 5.20 (a) TEM image of isolated carbon nitride NRs obtained by LP-PLA in 25% ammonia solution (laser fluence at 50 mJ per pulse, t = 2 h). (b) TEM image of an incomplete carbon nitride flower (25% ammonia solution, laser fluence at 125 mJ per pulse, t = 10 h) formed by the coalesced NRs. The arrows highlight the channels between the shell and the core. (c) After drying for 12 h (sample conditions identical to that in (a)), numerous aligned NRs form the framework of the flower. (e) Grass-like structure constructed from many protruding NRs (25% ammonia solution, laser fluence at 75 mJ per pulse, t = 3 h, drying at CPD). (f) Stem-like structure consisting of vertical NR branches (region highlighted by black box), sample conditions identical to that in (a), but with drying in a sealed tube. (g) After 24 h drying, the NRs have restructured to form 3D shapes [30].

The morphology of the self-assembled nanostructures is strongly dependent on the 'contruction' method. By applying different building blocks, different final complex architectures on various scales can be achieved. For lower ammonia concentration (25%), the carbon nitride formed 1D elongated nanoneedles or NRs. For low laser power (50 mJ) and short ablation time (2 h), the product contained

mostly a sparse collection of these isolated NRs (Figure 5.20(a)). However, with increasing laser power (125 mJ) and ablation time (10 h), the concentration of NRs increased, and in some regions they began to coalesce into incomplete flowers (Figure 5.20(b)). The radial distribution of the NRs formed channels leading from the centre of the flower to the edge. These channels may form the conduits along which the NPs diffuse outwards. When a droplet of the suspension, identical to that shown in Figure 5.20(a), was deposited on the substrate and dried for 12 h in a sealed tube, the carbon nitride produced flower-like structures constructed from pronounced tapered NRs (Figure 5.20(c)), instead of flowers made by the nanopetals (see Figure 5.17(a)). Typical NR building blocks with a rod diameter of 10-20 nm are shown in Figure 5.20(d).

A new morphology was also observed when the carbon nitride was created using a laser power of 75 mJ for 3 h ablation and placed onto a silicon substrate, and then dried in a critical point dryer (CPD). Figure 5.20(e) suggests that the product has a grass-like shape consisting of well-defined, protruding, short NRs. These structures can be assigned to the second class of morphology, mentioned previously in section 5.2.1. In contrast, if the substrate was dried in a sealed tube (water evaporation time ~8 h), the individual NRs vertically assembled into bundles (see the highlighted black box region in Figure 5.20(f) and formed stem-like structures. When the evaporation time of the liquid was increased to 24 h, the NRs developed a more complicated 3D structure, as shown in Figure 5.20(g). A possible explanation is that the longer time for evaporation of liquid allows sufficient time for the diffusion of all the NPs out of the flowers, leaving some liquid trapped in the gaps between the NR framework. With prolonged time, the wet NR framework has the opportunity to recrystallise or restructure into the shapes shown in Figure 5.20 (f-g).

More images of the symmetric organisation can be obtained by FE-SEM analysis, as shown in Figure 5.21. Figure 5.21(a) and (b) (sample synthesis conditions identical to those for Figure 4.29(a) in Chapter 4) give further evidence for type (I) organization (see Chapter 4.4.2.1 for three types of nanoleaf organization), *i.e.* the NPs have attached side-by-side and have fused into the surface of the leaf-like structures (Figure 5.21(b)). Such arrangements were observed following a very quick drying process, for example, drying in an oven or on a

hotplate in less than an hour. In contrast, if the substrate was dried inside a sealed tube (water evaporation time ~8 h or longer), the individual NRs vertically assembled into bundles (see the highlighted box region in Figure 5.21(c)) and formed leaf-like structures. Such NR bundles are similar to those shown in Figure 5.20(f). Surprisingly, when the evaporation time of the liquid was increased to 12 h, these NRs appeared to be 'interwoven' together into a lattice-like framework (Figure 5.21(d)) - yet the NRs were still aligned along the *c*-axis direction of the final complex architectures. These structures can be assigned as type (II), mentioned in Chapter 4.4.2.1.

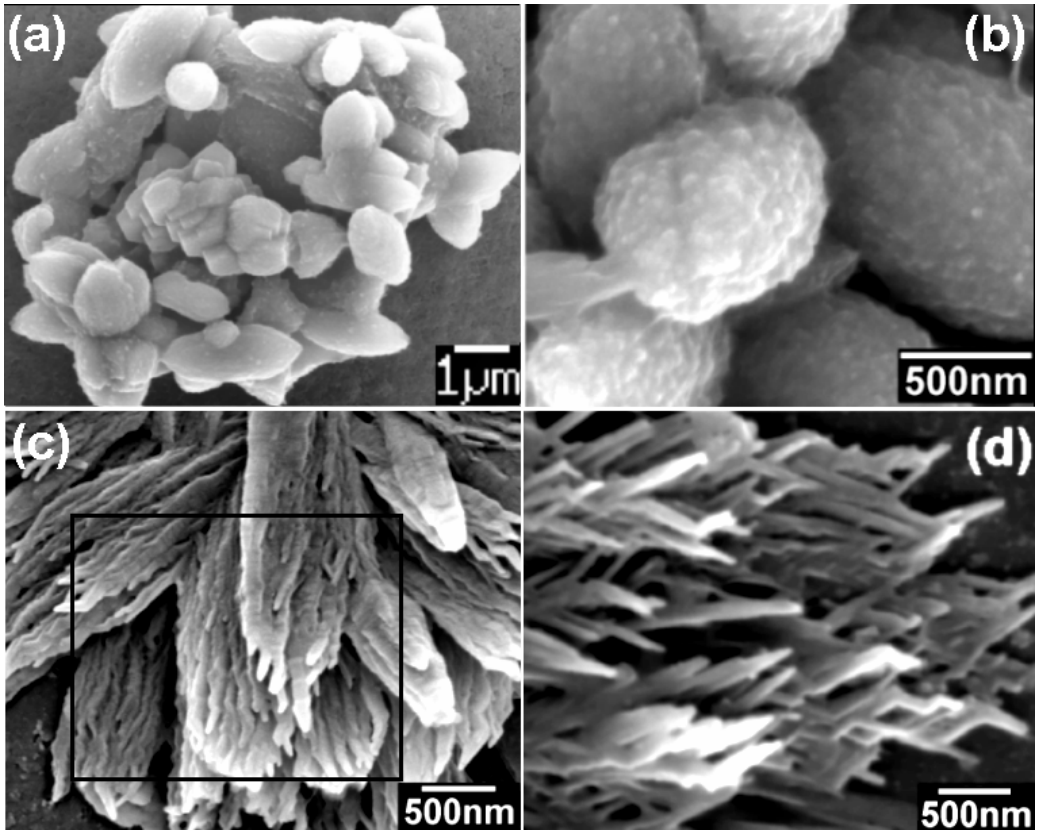

Figure 5.21 SEM images of (a) nanoleaf aggregates (sample conditions identical to that in Figure 4.29(a), TEM image shows leaf-like unit formed from numerous small NPs). (b) 3D leaf-like crystals with apparent NPs close-packed on the surface. (c) Leaf-like structures consisting of vertical NR branches (region highlighted by black box). (d) Interwoven NR arrangements to construct the final superstructures.

Thus, by combining LP-PLA techniques with bottom-up self-assembly seeded growth, 3D complex well-arranged carbon nitride architectures can be created, with their structures and spatial organisation with respect to the substrate controlled by the deposition and drying conditions. The synthetic approach described above can also be extended to a range of other solid materials. Further research in this area could be very interesting. A key advantage afforded by this aqueous multistage approach is the ability to systematically generate and control a diverse array of structures from a simple and inexpensive chemical route. With this improved understanding, LP-PLA may provide versatile and powerful industrial scale production processes for assembling complex architectures by specific design.

§ 5.4 General discussion about self-assembly mechanism

Our results clearly indicate that the formation of 2D or 3D hierarchical complex architectures is evaporation-driven self-assembly [46]. Evaporation-driven self-assembly is one of the most promising techniques for practical use [47], because it is inexpensive, has a high throughput, and it is a suitable technique for both low-dimensional assemblies and long-range-ordered complex structures. Various factors in our system, such as the rate of evaporation, the starting seed solution, and the size and the quantity of nanocrystals within the droplet, are very important to determine a well-defined self-assembly.

The formation of carbon nitride fully 3D structures was a slow process. During the evaporation process, capillary forces arise. At the edge of the meniscus, the thickness of a liquid film becomes small. The meniscus between particles has an unstable form in the thin liquid film (Figure 5.22). There are strong attractive interactions among the colloidal particles because of this instability. The attractive capillary force is called the ‘lateral capillary force’.

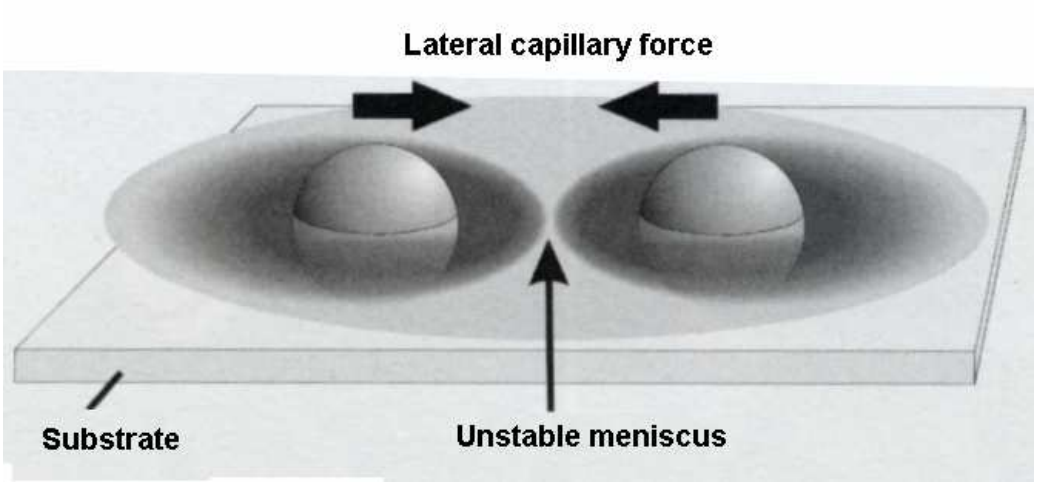

Figure 5.22 Schematic image of the lateral capillary force caused by an unstable meniscus, from ref.[48].

When the liquid evaporation rate is high, the liquid from the bulk suspension flows to the edge of the meniscus, and other particles in the suspension are driven toward this nucleus by the resulting convective transport (Figure 5.23). As in our system, the droplet was composed of carbon nitride solid objects floating at the silicon substrate interface, which interact by lateral capillary forces. Such forces might direct the patterning of the wettability of the surfaces via self-assembly minimization of the interfacial free energy of the liquid-liquid interface [49]. Clearly, the morphology transformation process of NPs to hierarchical architectures requires a significant degree of mobility in the local environment [50], which could explain why the well-defined flower-like or grass-like structures are only formed during a slow drying process. Similarly, the diffusion of the building blocks and the interconnection between the big structures are also related to such motion of the liquid flux. A high concentration of starting seed solution contained more components within the droplet may induce more interaction between the nanocrystals and increase the chance for the self-organization of aggregates in the later stage. This system was discussed in Section 5.2.3.

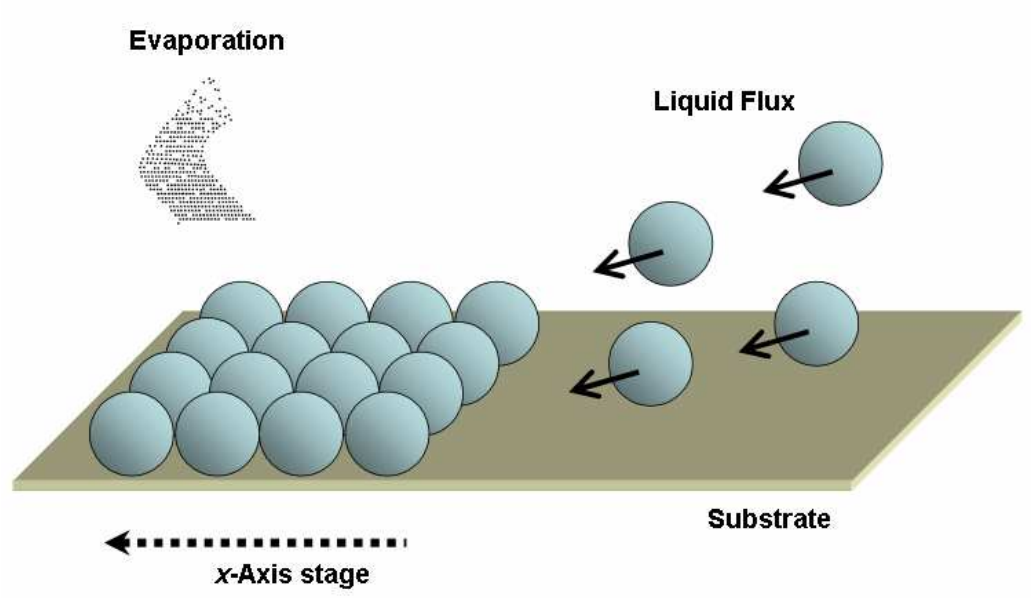

Figure 5.23 Schematic image of evaporation-driven self-assembly.

In self-assembly, the molecular structure determines the structure of the assembly [51]. Therefore, it is believed that the self-assembly into functional structures can be fabricated through design of the various components. Our results in section 5.2.3.2 have shown that the different shape of the starting components leads to the formation of different structurally defined aggregates. For example, the leaf-like seed solution imparted an asymmetric structure to the self-assembled aggregates (Figure 5.13). However, the rod-like seeds generated rod-branches (Figure 5.14) or grass-like structures (Figure 5.15) depending on the conditions, where the original shape of the components remained intact. The more complicated the shape, the more difficult it is to predict the final form of any aggregate. Further in-depth understanding of such phenomenon is required in future research.

§ 5.5 Conclusions

The formation and morphological evolution of 2D or 3D carbon nitride hierarchical complex structures was studied in this chapter. A two-step strategy was

developed to control the final well-defined superstructures. In the first step, carbon nitride seed solutions were prepared by liquid-phase pulsed laser ablation, as described in Chapter 4. In the second stage the chosen seed solution was deposited onto a silicon substrate. Via controlling the rate of evaporation, the starting seed solution, the size and the quantity of nanocrystals within the droplet, it was possible to create dense nanospheres, highly-symmetric flowers, and uniform grass-like structures, respectively.

Because of the mobility in the local environment, the smaller building blocks (NPs) appeared to be mobile with respect to the larger structures (flowers), and diffused outward from the centre with longer drying times. Such diffusion created different degrees of hollow structure, including core-shell, semi-hollow, and hollow organization, which find applications in new technological areas. In addition, interconnection between the larger structures was also observed for slow evaporation processes. For dense nanospheres, the fusing of the pristine nanospheres was weak and they were easily separated. However, the nanoflowers with many protruding NRs had sufficient capacity for the component NRs to occupy the spaces within the nanoflowers and fuse the flowers together more stongly.

From studies of the dynamics of self-assembly formation, it seems that the morphology of the initial stage of the complex architectures (grass-like or flower-like) was small aggregates of compacted 15-20 nm-sized dense spherical particles. The self-organization in the later stage may be associated with thermal motion of the droplets, for example, the evaporation speed. Although the mechanism is still not fully understood yet, our experiments which compared drying time and starting seed solution indicated that self-assembly into functional structures can be achieved through the design of the various components. A slow drying process will favour an increase in the structural complexity.

The formation of 2D or 3D hierarchical complex architectures in this work seems to be an evaporation-driven self-assembly process. The beauty of this approach is its simplicity and efficiency. If combined readily with micrometre-scale film patterning strategies, such as microcontact printing [52], direct writing, or lithography, it should provide a convenient pathway to the formation of functional hierarchical devices. By varying the design of the building blocks, materials

combination, interfacial chemistry, and confining dimensions, we should expect to discover new materials properties.

Bibliography

[1] Whitesides G M, Grzybowski B, *Science*, 2002, **295**, 2418.

[2] Whitesides G M, Boncheva M, *Proc. Natl Acad. Sci. USA*, 2002, **99**, 4769.

[3] Brinker C J, Lu Y, Sellinger A, Fan H, *Adv. Mater.*, 1999, **11**, 579.

[4] Wang Z L, *Adv. Mater.*, 1998, **10**, 13.

[5] Ying J Y, Mehnert C P, Wong M S, *Angew. Chem. Int. Ed. Eng.*, 1999, **38**, 56.

[6] Tang Z Y, Kotov N A, Giersig M, *Science*, 2002, **297**, 237.

[7] Liu B, Zeng H C, *J. Am. Chem. Soc.*, 2005, **127**, 18262.

[8] Kempa K, Kimball B, Rybczynski J, Huang Z P, Wu P F, Steeves D, Sennett M, Giersig M, Rao D V G L N, Carnahan D L, Wang D Z, Lao J Y, Li W Z, Ren Z F, *Nano Lett.* 2003, **3**, 13.

[9] Duan X F, Lieber C M, *Adv. Mater.*, 2000, **12**, 298.

[10] Sun Y, Fuge G M, Fox N A, Riley D J, Ashfold M N R, *Adv. Mater.*, 2005, **17**, 2477.

[11] Yang H G, Zeng H C, *J. Phys. Chem. B*, 2004, **108**, 3492.

[12] Mirkin C A, Letsinger R L, Mucic R C, Storhoff J J, *Nature*, 1996, **382**, 607.

[13] Sun Y G, Gates B, Mayers B, Xia Y N, *Nano lett.*, 2002, **2**, 165.

[14] Li Y D, Li X L, Deng Z X, Zhou B C, Fan S S, Wang J W, Sun X M, *Angew. Chem. Int. Ed*, 2002, **41**, 333.

[15] Motte L, Billoudet F, Pileni M P, *J. Phys. Chem.*, 1995, **99**, 16425.

[16] Maillard M, Motte L, Pileni M P, *Adv. Mater.*, 2001, **13**, 200.

[17] Liu B, Zeng H C, *J. Am. Chem. Soc.*, 2004, **126**, 8124.

[18] Petit C, Legrand J, Russier V, Pileni M P, *J. Appl. Phys*, 2002, **91**, 1502.

[19] Ngo A T, Pileni M P, *Adv. Mater.*, 2000, **12**, 276.

[20] Liu J P, Huang X T, Li Y Y, Sulieman K M, He X, Sun F L, *J. Mater. Chem.*, 2006, **16**, 4427.

[21] Liu B, Zeng H C, *J. Am. Chem. Soc.*, 2004, **126**, 16744.

[22] Lu Q F, Zeng H B, Wang Z Y, Cao X L, Zhang L D, *Nanotechnology*, 2006, **17**, 2098.

[23] Yang L, May P W, Yin L, Brown R, Scott T B, Ch*em. Mater.*, 2006, **18**, 5058.

[24] Yang L, May P W, Yin L, Scott T B, Smith J A, Rosser K N, *Nanotechnology*, 2006, **17**, 5798.

[25] Yang L, May P W, Yin L, Huang Y Z, Smith J A, Scott T B, *Nanotechnology*, 2007, 18, 335605.

[26] Wang J B, Zhang C Y, Zhong X L, Yang G W, *Chem. Phys. Lett.*, 2002, **361**, 86.

[27] Sounart T L, Liu J, Voigt J A, Hsu J W P, Spoerke E D, Tian Z, Jiang Y B, *Adv. Funct. Mater.*, 2006, **16**, 335.

[28] Liu A Y, Cohen M, *Science*, 1989, **245**, 841.

[29] Li J, Cao C B, Hao J W, Qiu H L, Xu Y J, Zhu H S, *Diamond Relat. Mater.*, 2006, **15**, 1593.

[30] Yang L, May P W, Huang Y Z, Yin L, *J. Mater. Chem.*, 2007, **17**, 1255.

[31] Sylvestre J P, Kabashin A V, Sacher E, Meunier M, *Appl. Phys. A*, 2005, **80**, 753.

[32] Pyatenko A, Shimokawa K, Yamaguchi M, Nishimura O, Suzuki M, *Appl. Phys. A*, 2004, **79**, 803.

[33] Rakshit R K, Budhani R C, *J. Phys. D*, 2006, **39**, 1743.

[34] Wang J B, Lei J L, Wang R H, *Phys. Rev. B*, 1998, **58**, 11890.

[35] Brinker C J, Lu Y F, Sellinger A, Fan H Y, *Adv. Mater.*, 1999, **11**, 579.

[36] Liu B, Zeng H C, *Small*, 2005, **1**, 566.

[37] Penn R L, Banfield J F, *Science*, 1998, **281**, 969.

[38] Lu T R, Kuo C T, Yang J R, Chen L C, Chen K H, Chen T M, *Surf. Coat. Tech.*, 1999, **115**, 116.

[39] Zimmerman J L, Williams R, Khabashesku V N, Margrave J L, *Nano Lett.*, 2001, **1**, 731.

[40] Likhacheva A Y, Paukshtis E A, Seryotkin Y V, Shulgenko S G, *Phys. Chem. Miner.*, 2002, **29**, 617.

[41] Liu A Y, Cohen M L, *Phys. Rev. B*, 1990, **41**, 10727.

[42] Zhang Z P, Shao X Q, Yu H D, Wang Y B, Han M Y, *Chem. Mater.*, 2005, **17**, 332.

[43] Motte L, Courty A, Ngo A T, Lisiecki I, Pileni M P, *Self-organization of Inorganic Nanocrystals, Nanocrystals Forming Mesoscopic Structures*, Pileni M P (ed.), Wiley-VCH Verlag GmbH & Co. KGaA, 2005, Weinheim, Germany, p.34.

[44] Wang C M, Pan X Q, Rühle M, Riley F L, Mitomo M, *J. Mater. Sci.*, 1996, **31**, 5281.

[45] Li Z Q, Xiong Y J, Xie Y, *Nanotechnology*, 2005, **16**, 2303.

[46] Maenosono S, Okubo T, Yamaguchi Y, *J Nanoparticle Res.*, 2003, **5**, 5.

[47] Salamanca J M, Ciampi E, Faux D A, Glover P M, McDonald P J, Routh A F, Peters A C I A, Satguru R, Keddie J L, *Langmuir*, 2001, **17**, 3202.

[48] Matsushita S, Onoue S Y, *Three-dimensional self-assemblies of nanoparticles, Nanocrystals Forming Mesoscopic Structures*, Pileni M P (ed.), Wiley-VCH Verlag GmbH & Co. KGaA, 2005, Weinheim, Germany, p.140.

[49] Bowden N, Terfort A, Carbeck J, Whitesides G M, *Science*, 1997, **276**, 233.

[50] Li M, *PhD thesis*, University of Bristol, 2000, pp. 132.

[51] Whitesides G M, Simanek E E, Gorman C B, *Nano Advanced Study Institute on Chemical Synthesis: Gnosis to Prognosis*, eds. Chatgilialoglu C, Snieckus V, 1996, Kluwer, Dordrecht, Netherlands, pp. 565-588.

[52] Jeon N, Finnie K, Branshaw K, Nuzzo R, *Langmuir*, 1997, **13**, 3382.